How electronic superpositions drive nuclear motion following the creation of a localized hole in the glycine radical cation

Cite as: J. Chem. Phys. (in press) (2022); https://doi.org/10.1063/5.0093780
Submitted: 30 March 2022 • Accepted: 24 May 2022 • Accepted Manuscript Online: 24 May 2022

Don Danilov, Thierry Tran, Michael J. Bearpark, et al.

Accepted to J. Chem. Phys. 10.1063/5.0093780

How electronic superpositions drive nuclear motion following the creation of a localized hole in the glycine radical cation

Don Danilov[2a], Thierry Tran[1,2b], Michael J Bearpark[2c], Jon P Marangos[3e], Graham A Worth[1d], and Michael A Robb[2f]

[1] *Department of Chemistry, University College London, 20 Gordon St., WC1H 0AJ London, United Kingdom*

[2] *Department of Chemistry, Imperial College London, Molecular Sciences Research Hub, 82 Wood Lane, W12 0BZ, London, United Kingdom*

[3] *Department of Physics, Imperial College London, Blackett Lab, Prince Consort Road, SW7 2BW, London, United Kingdom*

ORCID and mail:

[a]0000-0001-7843-5651	d.danilov20@imperial.ac.uk
[b]0000-0002-0722-0159	thierry.tran.18@ucl.ac.uk
[c]0000-0002-1117-7536	m.bearpark@imperial.ac.uk
[d]0000-0002-2044-4499	g.a.worth@ucl.ac.uk
[e]0000-0001-7169-6955	j.marangos@imperial.ac.uk
[f]0000-0003-0478-8301	mike.robb@imperial.ac.uk

Abstract

In this work we have studied the nuclear and electron dynamics in the glycine cation starting from localized hole states, using the Quantum Ehrenfest (QuEh) method. The nuclear dynamics is controlled both by the initial gradient and by the instantaneous gradient that results from the oscillatory electron dynamics (charge migration). We have used the Fourier transform (FT) of the spin densities to identify the 'normal modes' of the electron dynamics. We observe an isomorphic relationship between the electron dynamics normal modes (ED-NM) and the nuclear dynamics, seen in the vibrational normal modes (Vib-NM). The FT spectra obtained this way show bands that are characteristic of the energy differences between the adiabatic hole states. These bands contain individual peaks that are in one-to-one correspondence with atom pair (+ •) ↔ (• +) resonances (APR), which in turn stimulate nuclear motion involving the atom pair. With such understanding we anticipate 'designer' coherent superpositions that can drive nuclear motion in a particular direction.

INTRODUCTION

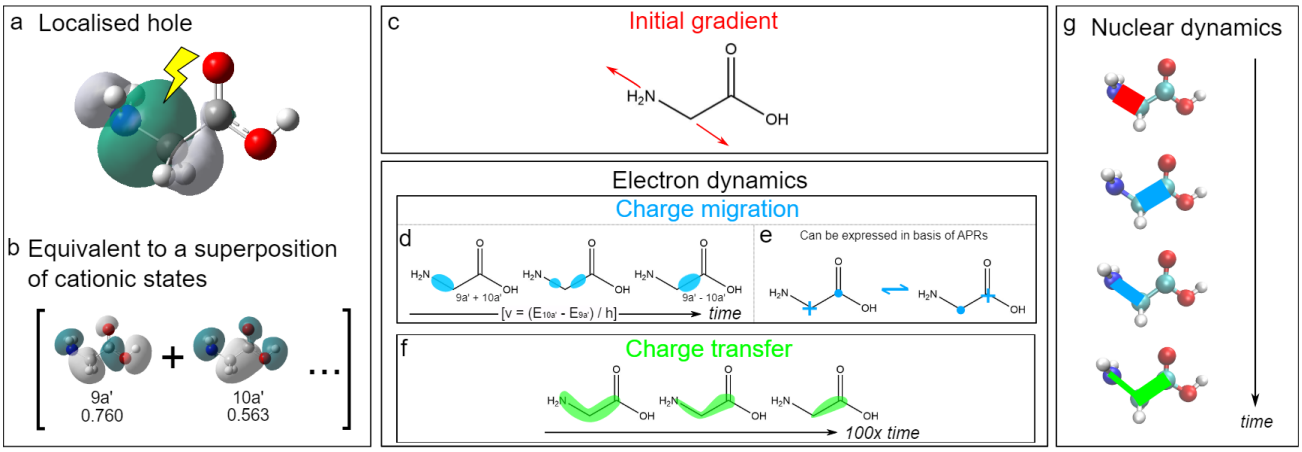

Scheme 1

In Scheme 1 we present a pictorial summary of the processes described in this paper. Our aim is to present an overview of the mechanisms (panels c-f), their origins (panels a-b) and consequences for nuclear dynamics (panel g) that result from the creation of a localized hole in the C-N bond.

The localised C-N hole state (panel a) can be described as either a single configuration state function with all bonding orbitals doubly occupied except for C-N (which is singly occupied), or as a superposition of adiabatic eigenstates that might be populated in a laser experiment (panel b). The C-N bond corresponds (mainly) to an in-phase superposition of the adiabatic states 9a' and 10a'. Note that the out-of-phase combination of 9a' and 10a' corresponds to a localized C-C bond hole.

The initial gradient (force on the nuclei) is shown in panel c and is directed along the C-N bond. Thus, the initial nuclear dynamics will involve relaxation of the C-N bond. In panel g we indicate this change in the geometry with time, with colour-coding: the initial C-N elongation is shown as a red line.

Because the C-N bond hole state is not an eigenstate, we will see charge migration illustrated in panel d. The hole oscillates between the C-N and C-C bonds. Equivalently, the oscillation is between combination of adiabatic states 9a'+10a' (CN bond hole state) and 9a'-10a' (C-C bond hole state) at a frequency which corresponds to the energy difference of the two adiabatic states [E(10a')-E(9a')]/h. The temporary population of a C-C bond hole state creates an instantaneous gradient along the C-C bond, which will stimulate nuclear motion involving the C-C stretch as shown in panel g.

When the localized hole creates a superposition of more than two states, it is convenient to resolve the electron dynamics into atom pair resonances (APR), one of which is shown in panel e. We can then follow the dynamics using the spin density, projected onto atomic sites. This directly relates the electron dynamics (reflected in the basis of APR) to the relative nuclear motion of a pair of atoms. Thus, the oscillation of the spin density associated with an atom pair resonance is in 1:1 correspondence with the change of distance between

the pair of atoms. We can see from panel e where the C-C atom pair resonance is correspondence with the change in the C-C bond length, seen in panel g, even though the initial hole was created in the C-N bond.

Finally, at longer times the charge migration, becomes biased in favour of the C-C bond (panel f). In the nuclear dynamics (panel g) the green line segment illustrates the effect of charge transfer: the C-N elongation becomes flattened, while the C-C elongation increases. Fundamentally, charge migration and charge transfer both describe motion of electrons that can be grouped under the collective description of electron dynamics. The difference is one of timescale (charge transfer is orders of magnitude slower than charge migration).

The first experiments to probe adiabatic ionized states in molecules were the ultraviolet photoelectron spectroscopy pioneered by Vilesov[1] and further developed by Turner[2]. These experiments offered an insight into the electronic structure and through Koopmans' theorem[3] relate the ionized adiabatic states to molecular orbitals. Furthermore, since an ionized state must relax after ionization, the effects of this relaxation could be seen as vibrational fine structure in the spectrum. In this article we explore coupled electron and nuclear dynamics and the electronic oscillations following molecular ionisation that are becoming accessible experimentally.

A central objective of modern attochemistry is the electronic control of the dynamics of molecules by population of a coherent superposition of excited states[4]. Short X-ray pulses, of sub-femtosecond duration, which are now available from high harmonic generation[5,6] and XFELs[7] can have sufficient bandwidth to create these superpositions. The difficulty is that such high bandwidth X-ray pulses will populate *all* possible superpositions within the laser pulse bandwidth assuming, as is usually the case, that the photoionization cross-sections of the neutral states are more or less the same[8]. One solution may be to implement selective probing of a single superposition of interest by using the core-to-valence resonant X-ray absorption scheme proposed[9] in 2014. This was recently demonstrated using two-colour XFEL pulses[10] to allow the dynamics ensuing from the superposition of a single hole state and (relatively) close lying shake-up satellite states to be isolated and monitored. With the intense two-colour attosecond pulses now available there is sufficient bandwidth (up to ~ 10 eV) to create and probe superpositions like the singly ionized states of the glycine molecule discussed in this paper.

A wavefunction corresponding to a coherent superposition of adiabatic electronic states is not an eigenstate and thus the wavefunction will evolve in time as a solution of the time-dependent Schrödinger equation. If the electronic wavefunction $\Psi(t)$ is expressed in the basis of adiabatic states $\phi_k\left(q;Q(t)\right)$ with complex coefficients $z_k(t)$ at nuclear geometries $Q(t)$ and q the electronic co-ordinates, we have

$$\Psi\left(q,t;Q(t)\right)=\sum_{k=1}^{N} z_k\left(t\right)\exp\left[-iE_k\left(Q(t)\right)t\right]\phi_k\left(q;Q(t)\right) \qquad [1a]$$

Equation 1a depends parametrically on $Q(t)$ at each time-step. The $z_k(t)$ are complex time-dependant coefficients. Therefore, the electronic Hamiltonian is parameterized by $Q(t)$ and varies slowly.

To proceed further with our analysis we will make a two-state simplification as documented elsewhere in literature[11,12]. This allows us to analyze electron dynamics of all states in a pairwise way. However, it is an approximation since cross term states from 3 (or more) simultaneous state interactions could play a role in the full electronic superposition and the dynamics that result. In our calculations, the only interactions of significant intensity are those that arise from pairs of states. We drop the explicit parametric dependence on $Q(t)$ in the formulae for simplicity, then we can write the time-dependent wavefunction, expanded in the basis of the two eigenstates,

$$\Psi(t)=z_1(t)e^{-iE_1(t)t}\phi_1(t)+z_2(t)e^{-iE_2(t)t}\phi_2(t) \qquad [1b]$$

Where the time-dependence of the energies is due to the dependence on moving nuclei. The probability density derived from Eq 1a can be shown to be[11,12]

$$\left|\Psi(t)\right|^2=\left|z_1(t)\right|^2\left|\phi_1(t)\right|^2+\left|z_2(t)\right|^2\left|\phi_2(t)\right|^2+2\,\mathrm{Re}\left(z_1(t)^*z_2(t)e^{i(E_1(t)-E_2(t))t}\phi_1(t)^*\phi_2(t)\right) \qquad [1c]$$

The oscillatory terms of the form $\left(z_1(t)^* z_2(t) e^{i(E_1(t)-E_2(t))t} \phi_1(t)^* \phi_2(t)\right)$ are the quantum mechanical origin of the charge migration. Whether we see dynamics associated with a pair of states depends on the magnitudes of z_1 and z_2. In practice, we see results consistent with the products of $z_1 z_2$. Invoking the Planck – Einstein relation ($E = h\nu$) we would then expect oscillations to occur at characteristic frequencies as a function of the energy gap between adiabatic states.

$$\nu = \frac{E_2 - E_1}{h} \qquad [1d]$$

This electron dynamics generates instantaneous gradients at the turning points, driving the nuclear motion. In a recent paper on the benzene radical cation Tran *et al*.[13] have exploited the high symmetry environment to demonstrate the isomorphism between the electron dynamics and nuclear dynamics.

By controlling the mixing of the electronic states, one can change the electron dynamics and thus control subsequent nuclear dynamics. Glycine possesses a much lower symmetry environment, and as such in lieu of analytic algorithms we must opt for a more numerical approach. The presence of heteroatoms with lone pairs further complicates the description of the electron dynamics since the hole may now occupy non-bonding orbitals.

How can one choose such superpositions? For superpositions of vibrational wavefunctions alone i.e. nuclear dynamics, one might use some sort of fitting procedure. In this work, recognizing that coherent superpositions lead to localization, we shall select the starting state in such a way that the superposition corresponds to the ionization from a localized bonding molecular orbital. In this way the initial gradient ought to be localized.

For this study of the glycine cation, we shall use the Natural Bonding Orbitals (NBOs) localisation scheme of Weinhold *et al.*[14] In a 2018 paper Polyak *et al.*[15] used this scheme on the glycine cation for a discussion of the ionization out of the carbonyl sigma bond and subsequent decoherence of the electron dynamics. We will use the same NBOs that were used in that work, as shown in Figure 2.

In Figure 2, the connection between the localized hole states (columns) and adiabatic states (rows) can be understood with an example; NBO8 is a state where the single electron is localised in the C-N bond. It corresponds to a superposition dominated by CI_5 and CI_6 adiabatic states (spectroscopically labelled 10a' and 9a'). Dynamics between these states (indicative of a coupling) was experimentally observed by Schwickert et al.[16] The comparison is not perfect as their experiments involve the coupling of 9a' and 10a' states to shakeup states (1h + 2h1p), which involve excitation and ionisation. Where the notation 1h signifies a single excited hole state and 2h1p signifies double hole excitation + 1 particle (electronic) excitation as is the standard nomenclature. These states are not considered in our calculations due to our choice of orbital active space. Looking at the CI_5 and CI_6 rows, suggests a strong coupling between the C-N (NBO8) and C-C (NBO6) localised bond holes in addition to one O[3] lone pair hole (NBO2). The coupling between localised orbitals that is associated with the electron dynamics is dominated by the $V_{ij}^{nuc-elec}$ nuclear-electron attraction integral associated with orbitals i and j, and the nuclei a

$$V_{ij}^{nuc-elec} = \sum_a \int \psi_i(\mathbf{r}_{1a}) \left(\frac{1}{r_{1a}}\right) \psi_j(\mathbf{r}_{1a}) d\mathbf{r}_{1a}$$

Thus, qualitatively the coupling is related to the one-electron attraction of the overlap density (or crudely the interpenetration of the orbitals). Thus, NBO i and NBO j are coupled via the overlap density $\psi_i(\mathbf{r}_{1a})\psi_j(\mathbf{r}_{1a})$ Since these bonds are adjacent, the $V_{ij}^{nuc-elec}$ term will be large because of the overlap charge density of the orbitals. As we will see shortly, ionization of the C-N generates electron and nuclear dynamics involving the C-C bond. Furthermore, since NBO8 is dominated by the CI_5 and CI_6 adiabatic states we should see a characteristic electron dynamics frequency (Eq 1c) at $(E_6 - E_5)/h = 1.06 \times 10^{15}$ Hz ~ 1 PHz.

The electron dynamics of glycine has been extensively studied by Kuleff et al.[17] who demonstrated rapid oscillation of the hole over the molecule, with frozen nuclei. Their paper hinted at the possibility that nuclear motion may trap the hole, and as we shall shortly discuss, we see this effect in our data. In a recent work, Delgado et al[18] reported on the evolution of nuclear geometries as a function of chosen starting pure adiabatic states. In this work we will start from localized hole states which correspond to superpositions of these adiabatic states. Lara-Astiaso et al[19,20], using TD-DFT, suggested that ionisation out of a Kohn-Sham orbital leads to negligible nuclear motion for the first 8 fs. In contrast, the complex superpositions of adiabatic states with which we shall start our dynamics do not follow this rule.

Two limiting forms of electron dynamics have been identified in cationic systems – charge migration and charge transfer[21]. The former is characterized by ultrafast oscillations (possessing a frequency on the scale of 10^{15} Hz) (Scheme 1d) whereas the latter is a more permanent translocation of charge (occurring on the time scale of several femtoseconds) (Scheme 1f). Charge transfer can be effectively described as a limiting case of charge migration where the charge oscillation has such a long time period the charge effectively never returns to original positions. Thus, for charge migration (as discussed by Cederbaum[22]) for 2 atomic centres A, B involves dynamic oscillation between (A+ B•) ↔ (A• B+) with approximately equal weight. For charge transfer we have a permanent shift of equilibrium between the oscilating forms to yield e.g. [20%] (A+ B•) ↔ (A• B+) [80%]. As we shall discuss in detail, we can track the electron dynamics corresponding to charge migration via the oscillatory behaviour of the spin density projected onto the atoms[23].

In this work we will look at the electron dynamics (and subsequent nuclear dynamics) of the inner valence shell electrons (σ rather than π bonds) of glycine cation (Figure 1). By perturbing the σ bonds, we should see a direct effect of the electron dynamics on nuclear motion. We shall make this connection by examining the Fourier Transform (FT) of the spin density projected onto atoms. Before discussing the theory and the results we pause to give a brief overview.

Analysing the FT of this oscillating spin density, one obtains a spectrum characteristic of the initial coherent superposition of states. The bands in this spectrum correspond to the “normal modes” of the electron dynamics. We refer to these as normal modes because they have a characteristic frequency, given by Eq 1d (i.e. they are quantized). These ED-NM, in turn drive the nuclear dynamics (vibrational normal modes, Vib-NM). The charge transfer electron dynamics cannot be seen directly in this spectrum because it is too slow; however, we can see the small changes in the frequencies of the ED-NM caused by charge transfer.

We can describe these ED-NM as linear combinations of resonance pairs (+ •) ↔ (• +) of 2 atoms (as in H_2^+ [24]). We shall refer to these as atom-pair resonances (APR), analogous to the way that one describes the Vib-NM as combinations of bond stretches and angle changes. This will be discussed in detail in Figure 3 subsequently. These APR give rise to pairs of anti-symmetric peaks in FT spectra (there are also symmetric pairs, which are a consequence of electron dynamics of atoms mutually involved in other resonance modes).

However, in the FT bands we can only identify the component pairs of atoms contained in the corresponding ED-NM. Thus, we only know the components (i.e. the APR) that are contained in the ED-NM, not the exact linear combination.

A useful comparison can be made with IR Spectroscopy where one has the absorption lines each associated with a Vib-NM but not the constituent nuclear deformations. Using isotope substitution, one might identify the atoms associated with the absorption line, however, it is only by computing the vibrational normal modes and associated frequencies that one can make a full assignment. In contrast, we can identify the APR involved in the ED-NM bands in the FT spectra, but the APR may be present in multiple ED-NM.

If we identify a component atom-pair resonance, APR, in the spectra as a peak within a band, then we would expect to see a corresponding nuclear geometric deformation involving the same atoms. If the atoms are bonded, we will see a bond length change. If the 2 atoms are separated by an anchor atom, we will see a bond angle change. If we were to see 3 bands corresponding to two different ED-NM (Eq 1), we would expect to see 3 Vib-NM activated.

However, in a dynamics simulation this does not necessarily imply that these ED-NM are active contemporaneously. In the case of a charge transfer the APR composition of the ED-NM may change with time. There may also be several peaks within a band associated with the same APR. This of course implies a change in the weight of the atom-pair resonance with time, perhaps due to charge transfer.

Thus, looking at the individual bond (APR) components of the FT bands could be misleading; one might see an APR peak corresponding to a bond, but no bond extension. This would result from a symmetric and antisymmetric nuclear vibration Vib-NM each containing the bond in question, and which might cancel out the extension of that bond. Thus, it is the ED-NM and the Vib-NM that are isomorphic (in a 1:1 correspondence); but we can identify them through the APR that correspond to the peaks within the band.

We now elaborate on the evolution (broadening of the bands) of the ED-NM due to the effect of charge transfer and the change of the Vib-NM, with time. As time progresses, the ED-NM of the electron dynamics change in frequency and composition as the nuclei evolve in time. At the beginning we can have a situation that corresponds to charge migration (rapid oscillations in the spin density between pair of atoms on the scale of 10^{15} Hz). As the time evolves, we can have charge transfer (a permanent translocation of spin density from one atom to another). Thus, we will see the ED-NM peak frequencies (corresponding to the APR) change as a result. Of course, charge transfer would correspond to very low frequencies, so we do not see this effect directly in the FT spectra, rather we see the effect in the widening of the ED-NM bands resulting from the shifts in the peaks.

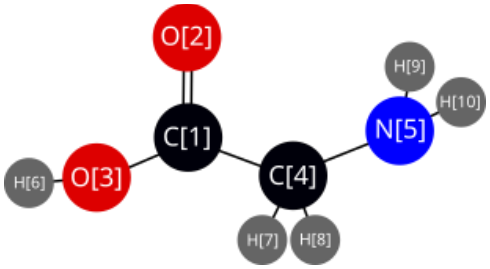

Figure 1 Numbering of atoms in glycine. For convenience, we shall use an Element [Atom Number] notation (e.g. O[2] to refer to the carbonyl oxygen)

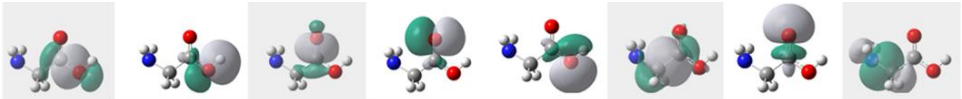

	NBO_1	NBO_2	NBO_3	NBO_4	NBO_5	NBO_6	NBO_7	NBO_8	Energy [eV]	Symmetry
CI_1	0.2216298	0.0120480	0.0019619	0.9201116	0.2175083	-0.2308964	0.0120945	-0.0579364	0.0	15a′
CI_2	0.1348270	-0.3551293	0.3891814	-0.0816426	0.5733370	0.3279627	0.4995947	0.1082014	3.9193	13a′
CI_3	0.5371606	0.3856132	0.0778165	-0.3426892	0.2377957	-0.5234704	0.1471610	-0.2950343	6.7584	11a′/12a′
CI_4	-0.0111017	0.4511562	0.3534264	0.1593372	-0.5368070	0.1660805	0.5735594	0.0363504	7.3375	12a′/11a′
CI_5	0.3755901	0.4853876	-0.0752225	0.0017301	0.1888725	0.4125462	-0.3070593	0.5634865	12.6553	10a′
CI_6	-0.0729007	-0.1761335	-0.0215735	-0.0599991	-0.0820381	-0.5755538	0.2087885	0.7602711	17.0542	9a′
CI_7	0.5093371	-0.4130587	0.5145817	-0.0143565	-0.4126581	0.0007593	-0.3662382	0.0232379	30.5127	7a′
CI_8	-0.4880885	0.2902704	0.6683189	0.0097930	0.2580243	-0.1899113	-0.3572446	0.0223633	33.9105	6a′

NBO_N is CSF where NBO-N is singly occupied … i.e. hole location

Figure 2 The starting 8SA-CASSCF(15,8) states and orbitals, converged from the 'small but complete subset of NBOs' suggested by Polyak et al[15], computed at the ground state (DFT-B3LYP/6-31G) geometry. The rows (labelled CI_i) represent the adiabatic states (the ϕ_i of Eq 1a). Their relative energies and spectroscopic labels are shown in the 2 rightmost columns. The other columns, labelled NBO_i correspond to a localised hole configuration state function (CSF), where the plotted orbital (top), is singly occupied. Reading down the column, the numbers are simply the z_i adiabatic state coefficients of Eq 1a for a localised hole state. Localised hole states that have high coefficients in the same adiabatic state are said to be strongly coupled. Likewise, if a localised state has multiple large adiabatic states those states are also said to be coupled.*

2) Theoretical and conceptual discussion

Spin density

The spin density, defined as the difference between densities of alpha and beta electrons, is projected onto atomic centres using the Mulliken populations. This allows us to track the single unpaired electron in Gly^+ and through its oscillations infer the location of the hole. We use the computational method for spin densities described by Polyak et al[23]. We have chosen this strategy because it depends only on the Ehrenfest wavefunction itself and not the details of the computations of NBO or optimization of the orbitals.

It is the rapid oscillations in the spin density (ED-NM), referred to as charge migration by Cederbaum[22] that are of great interest in how they drive nuclear motion. In this work we will identify these characteristic frequencies in FT spin density spectra (In contrast, a charge transfer takes place on a longer timescale and can be seen in a simple moving average of the spin density).

The ED-NM characteristic frequencies (Eq. 1) correspond to the bands in the FT spin density spectrum. Each of these bands contains peaks corresponding to atom-pair resonances (APR). Kauzmann[24] in his 1957 textbook described these oscillations in H_2^+ as an 'electronic tautomerism', connecting pairs of resonance forms.

We now discuss the APR for Glycine cation. We have restricted our computations to the 5 heavy atoms (via our choice of CASSCF active space and selection of vibrational normal nodes). All possible 10 potential APR are shown in Figure 3. The + indicates the location of the hole and the dot the location of the unpaired electron. These form a complete basis for a full description of the ED-NM. Note that only pairs of out of phase oscillations are of interest as they can lead to instantaneous gradients between the atoms involved in charge migration. The atom pairs oscillating in-phase are involved in other APR, and lead to gradients with those respective atom pairs.

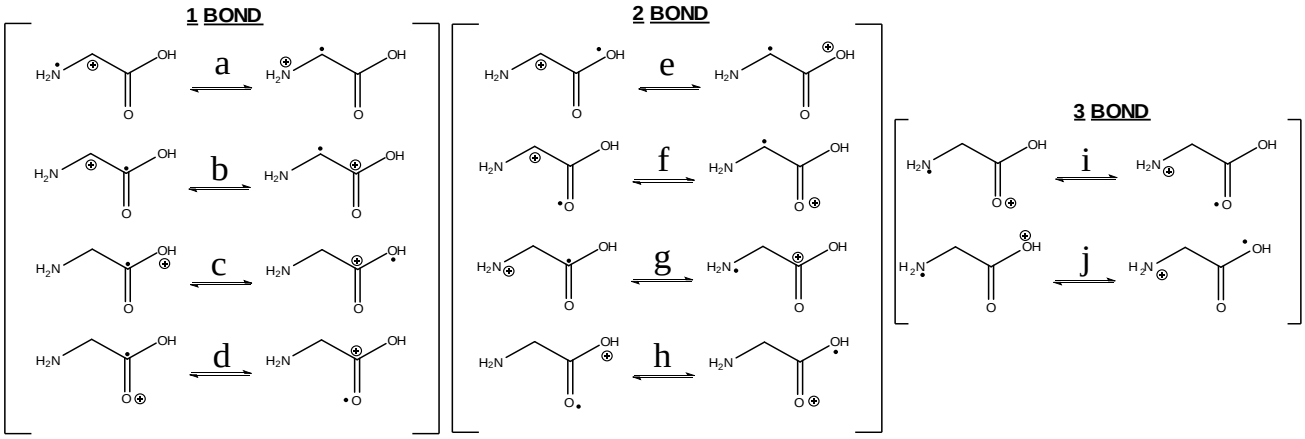

Figure 3 *All possible 2 heavy-atom pair resonances APR, grouped by number of bonds separating the oscillating components. We would expect activation of a 1 bond resonant pair to lead to a change in bond length across which the oscillation is occurring. 2 bond oscillations are expected to yield an activation of bending mode between the atoms. 3 bond resonances are expected to be significantly weaker and lead to dihedral angle bends (torsion).*

Fourier transform of spin density

To study oscillatory behaviour of the electron dynamics we have used the spin density projected onto atomic sites. We shall Fourier transform (FT) the raw time-dependant spin density data to study the frequencies of the electron dynamics and the analysis into APR contributions.

In their TD-DFT study of glycine[19], Lara-Astiaso *et al.* also used the FT of the spin density to study electron dynamics. The dynamics they observed were very weak since they started with stationary states. In contrast, we will show that the electron dynamics controls the nuclear dynamics and the peaks in the FT spectra can be used to correlate the population of ED-NM and Vib-NM.

The discrete FT, based on the Cooley–Tukey algorithm[25], as implemented in the NumPy package[26], for a given set of data $\{x_i, t_i\}$, yields a set of complex coefficients and associated frequencies: $\{z_i, f_i\}$. Typically, the square moduli $\{|z_i|^2, f_i\}$ are then reported as the power spectra. We also extract the phase information contained in the data. This is done by computing $\{\mathrm{sgn}(\arg(z_i))\cdot|z_i|^2, f_i\}$. This allows us to see both the relative intensities and the relative phases of the signals. To remove some of the noise and potentially erroneous peaks in the FT, we shall use a few signal processing techniques. First, we reverse the list: $\{x_i\} \to \{\overline{x_i}\}$ and then prepend the reversed list to the original list: $\{\overline{\overline{x_i}}\} = \{\overline{x_i}\} \oplus \{x_i\}$. This operation exploits time-symmetry to give more datapoints, stronger signals, and less noise. Finally, a zero-to-zero correction is applied where the new list is convoluted with a cosine function of the form $\cos\left[\frac{\pi t_i}{2t_{final}}\right]$ where t_{final} is the timestamp of the last datapoint.

This of course introduces a new frequency into the data (comparable to that of charge transfer). To remedy this issue, we discard the first 4 points of the FT spectra, corresponding to ultra-low frequencies and shall explore the slow (charge transfer) effects through the simple moving average plots instead.

In a FT spectrum we expect to see peaks in each heavy atom's spin density corresponding to a frequency at which it oscillates. These peaks point either up or down depending on the relative phase. The peaks are grouped into bands as the dynamics of the system will cause the exact frequencies to change (for static nuclei we would expect clear single peaks).

Pairs of atoms oscillating at the same frequency band can then be described as either in phase or out of phase based on their relative phases (if they point in the same direction they are in phase and vice versa).

If two atoms' spin density oscillates at a given frequency where they are out of phase, these atoms are said to be in an active atom-pair resonance (APR) shown in Figure 3. Each band is said to be an active ED-NM and can be expressed as a linear combination of its constituent APR.

To assign the spectrum we will introduce a shorthand notation where 2 sets of mutually out of phase oscillating sets of atoms are written either side of a double dash. For example, C[1] // O[2], O[3] indicates atom-pair resonances consistent with an activation of the C[1] ↔ O[2] and C[1] ↔ O[3] atom-pair resonances as shown in Figure 3cd. The presence of a component APR will correlate with a geometric atom-atom distortion.

3) COMPUTATIONAL DETAILS

The initial ground state geometry was optimized at the DFT-B3LYP/6-31G* level of theory.

The non-adiabatic dynamic simulations were preformed using the Quantum Ehrenfest (QuEh) method of Jenkins et al.[27]. This consists of 2 intertwined computations: the direct dynamics variational multiconfigurational gaussian wavepacket (DD-vMCG) algorithm[28] to drive the nuclear motion on a time-dependant Ehrenfest[29] potential energy surface.

The Ehrenfest wavefunction, nuclear gradients and Hessian were computed via the propagation of the electronic CAS-CI wavefunction as a solution of the time-dependent Schrodinger equation described by Vacher et al[29]. We used this algorithm as implemented in a development version of GAUSSIAN (Development version J05)[30]. For our computation we have selected an active space of 15 electrons in 8 orbitals (the same as the one used by Polyak et al[15]). In a single propagation step the orbitals are re-orthogonalized and the orbital rotations are performed to optimize the orbitals. The active orbital rotations are skipped since the energy is approximately invariant to such rotations. Thus, the NBO are kept effectively constant during the propagation (except for a small re-orthogonalization). Since the orbitals are not fully optimized the CP-MCSCF equations need to be solved to compute the gradients and hessians. Thus, the APR remain almost unchanged. However, our results are not sensitive to such details if we use spin densities for the analysis rather than weights of CI coefficients etc.

DD-vMCG propagates the nuclear wavefunction, using the gradient of the Ehrenfest state in a basis of moving gaussian wavepackets (GWPs) as implemented in the QUANTICS[31] package. The DD-vMCG algorithm requires a set of normal modes along which the GWPs are given an initial momentum and whose populations, positions and momenta are updated at each simulation step. We have selected a subset of 7 planar bond-length bond-angle deformations of the heavy atoms from the 24 normal modes yielding a total of 15 GWPs (2 per normal mode, plus one that begins in the centre with no momentum). The initial conditions used momentum sampling of the normal modes. These were computed at the DFT-B3LYP/6-31G* level of theory and are shown in Figure 4.

The evolution of the system was computed for 20 fs - this is to avoid instabilities associated with the large bond extensions leading to a breakdown of the orbital active space

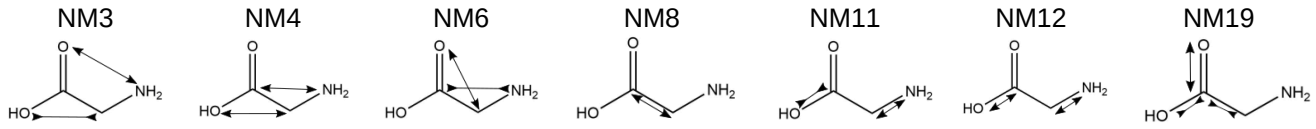

Figure 4 – Schematic diagrams of the 7 vibrational normal modes of glycine involving heavy atoms computed at DFT-B3LYP/6-31G level of theory chosen for evolution within the DD-vMCG simulation. These can be grouped into bends (NM3, NM4, NM6) and stretches (NM8, NM11, NM12, NM19).*

4) Results and discussion

In this section we will discuss ionization from the C-N bond (NBO8 in Figure 2). We the summarise the case for a hole in the C-C bond (NBO6), relegating the more detailed discussion to SI. We have studied two other similar cases (NBO1 and NBO3). The associated discussion is presented in the supplementary information.

NBO8 C[4]-N[5]

In this section we shall discuss the dynamics (electronic and nuclear) where the initial electronic wavefunction corresponds to a localised hole in NBO8 (the C-N bond). Examination of the CI transformation matrix (Figure 2 highlights) suggests that a localised C-N hole is composed primarily of the CI_5 and CI_6 adiabatic states. The corresponding rows of the matrix suggest a strong coupling between the C-N and C-C localised bond hole states. We should therefore expect electron dynamics between these 3 atoms; N[5], C[4] and C[1].

The computed changes in nuclear geometry over the course of simulation are displayed in Figure 5. The dominant effect is a C-N elongation, with a smaller C-C stretch and a C-C-N bond angle deformation. The NBO that are strongly coupled through adiabatic electronic states (Figure 2 C-N and C-C) are the ones

showing significant nuclear motion. As we shall discuss, the C-N extension is a manifestation of the initial gradient, whereas the other distortions are a result of electron dynamics (i.e. charge migration).

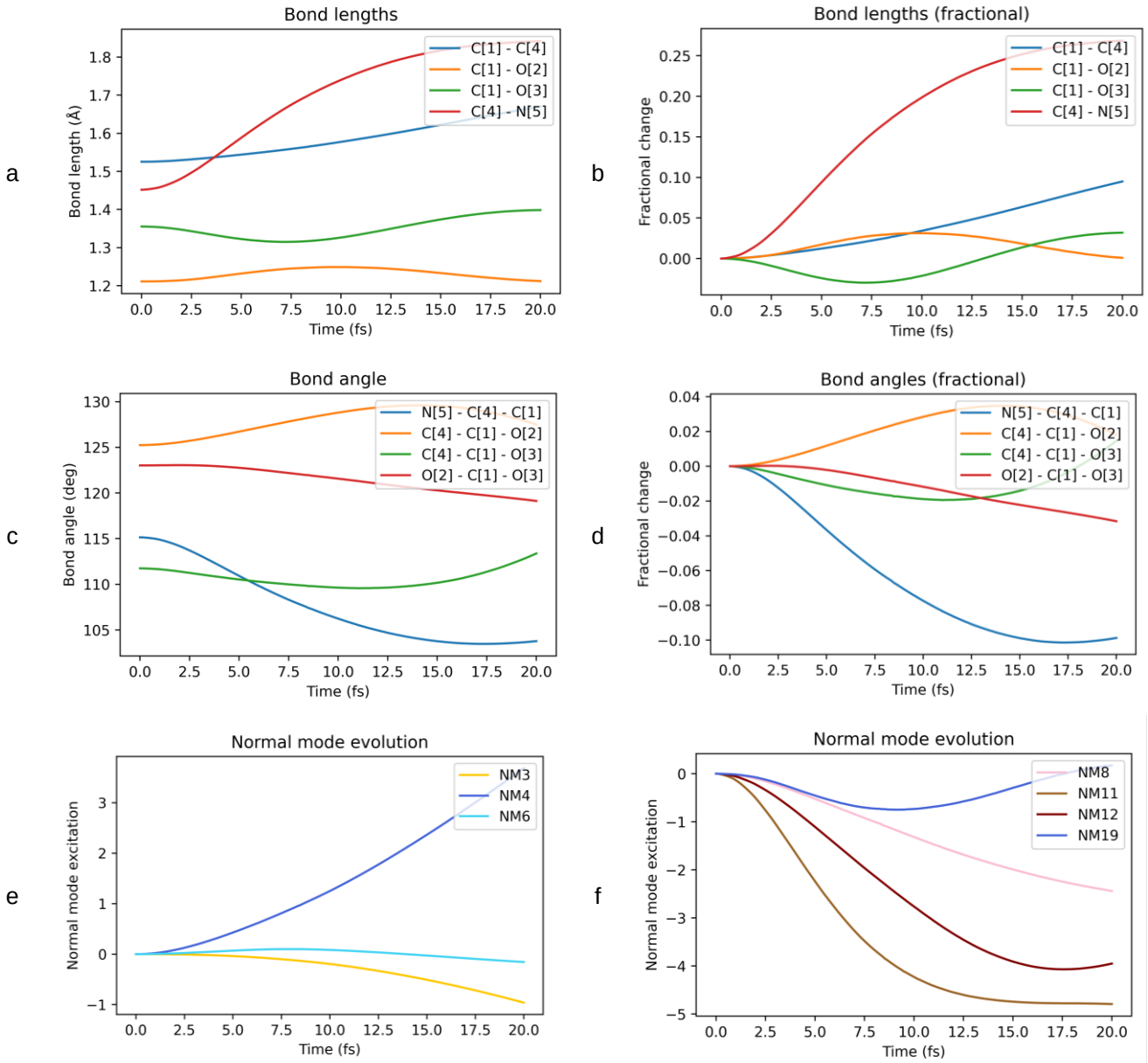

Figure 5 Major bond (a, b) and angle (c, d) evolutions and normal mode activations (split into bends (e) and stretches (f) for clarity), as a function of time for NBO8 starting state. Note the large C[4]-N[5] extension and a large N[5]-C[4]-C[1] angle bend activation

The first electronic effect to consider is that of an initial gradient. A localized hole in a bond should induce a localised initial gradient along that bond. This is shown in Figure 6. The initial motion in the dynamics must be controlled by the initial gradient. In Figure 5a,b we show the corresponding large C-N extension. Note that there is no gradient component along the C-C bond or the C-C-N bond angle, so these deformations must arise from the electron dynamics.

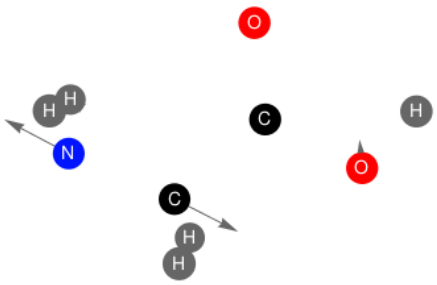

Figure 6 Initial gradient for NBO8 starting state

We now discuss the electron dynamics. As the hole oscillates it will generate a gradient at its turning points, nudging the nuclei. The spin density FT spectra (Figure 7) shows the presence of distinct peaks, suggesting that the ED-NM are quantized as linear combinations of APR (Figure 3). When they occur in any given system, they occur only at specific frequencies. In the FT spectra in Figure 7 we observe 3 distinct peak groups (i.e. bands) at 1.0 PHz, 1.3 PHz and 2.4 PHz we can describe these as C[4], N[5] // C[1], O[2], O[3], O[3] // N[5], C[4] and C[1] // O[3], N[5] using our double dash notation respectively. For example – in the 1.3 band we see O[3] (blue) oscillating out of phase with N[5] (cyan) and C[4] (orange).

Note that the 1.0 PHz band corresponds to an energy difference of ~4.1 eV. This aligns very closely with the CI_5/CI_6 gap of 4.4 eV with frequency $(E_5 - E_6)/h$. Likewise, the 1.3 PHz band would have an energy of ~5.4 eV which aligns well with the CI_4/CI_5 gap of 5.3 eV. Lastly the 2.4 PHz peak would have an energy of ~9.9 eV which closely matches the CI_4/CI_6 gap of 9.7eV. We now turn to a discussion of the individual component APR (Figure 3) of these ED-NM.

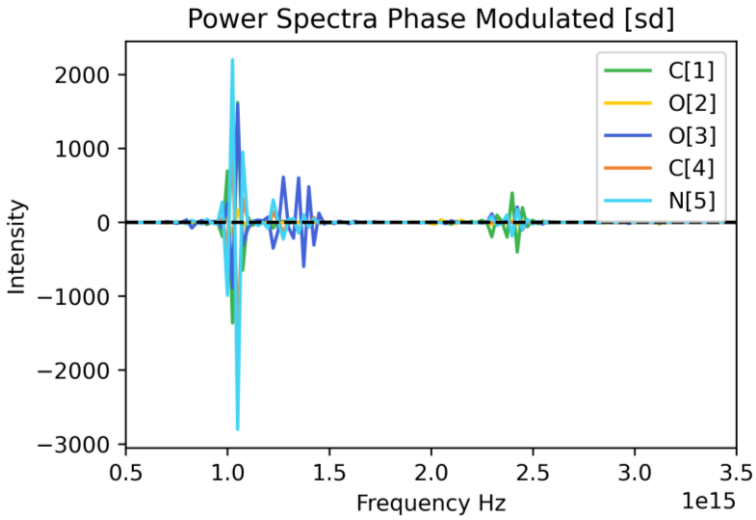

Figure 7 FT plot of the spin densities over the course of a 20 fs simulation starting with the hole localised in the C-N bond (NBO8). Atomic labelling is as shown in Figure 1. The possible pairs of atoms on the same side of the zero line are oscillating in phase together, out of phase with the atoms on the other side of the zero line. There are large peaks at 1.0, 1.3 and 2.4 PHz. The 1.0 PHz peak corresponds to electron dynamics we will label as C[4], N[5] // C[1], O[2], O[3]. Pairs of atoms either side of the double slash (//) are out of phase. The out of phase pairs correspond to activation of some of the associated APR shown in Figure 3. The 1.2 PHz band is a O[3] // N[5], C[4] while the 2.4 PHz band can be described as O[3], N[5] // C[1].

The FT spectra between heavy atoms contained in Figure *7* are replotted pairwise Figure 8. These are ordered based on atom number pairs C[1]:O[2], C[1]:O[3] etc. We shall focus on C[1] ↔ O[3], C[1] ↔ C[4], C[1] ↔ N[5], C[4] ↔ N[5] pairs. We do not report data for the other pairs (e.g. C[1] ↔ O[2]) because their intensities are relatively small.

We begin with the atom pair C[1] ↔ N[5] (APR Figure 3g) shown in Figure 8f. C[1] and N[5] are out of phase at 1.0 and 2.4 PHz and one can see the activation of corresponding NM4 activation (C-C-N angle

deformation) in Figure 5. Note too that N[5] is oscillating weakly at 1.3 PHz but C[1] is not – this is evidence of the N[5] being involved in ED-NM with other atoms. Also, in the raw spin densities (Figure 8e) there is a noticeable change in the spin density with time and this is a result of the charge transfer from N[5] to C[1] and will be addressed later. This charge transfer is in part responsible for the fact that there are several C[1] ↔ N[5] resonance frequencies in the same bands.

Now let us turn to the C[1] ↔ O[3], atom pair shown in Figure 8b (APR Figure 3c). The 3 peaks are present in the spectra; however, the 2 spin densities are in phase at 1.0 PHz, only O[3] is present in 1.3 PHz and the two are out of phase at 2.4 PHz. Because the intensity of the 2.4 PHz is small the associated resonance (APR Figure 3c) is relatively weak. Accordingly, we observe only a small C-OH bond length activation as shown in Figure 5.

In Figure 8d we show the FT data for C[1] ↔ C[4] (APR Figure 3b). Here we see only a large, strong, out of phase peak at 1.0 PHz. The 2.4 PHz peak is present for C[1] only and 1.3 PHz for C[4] only. Again, this indicates that these atoms are involved in other APR and associated ED-NM. The anti-symmetric peak band at 1.0 PHz for C[1] ↔ C[4] corresponds to resonance mode in Figure 3b. This, in turn, is consistent with the C-C bond elongation shown in Figure 5.

Finally, in Figure 8h we present the C[4] ↔ N[5] data (APR Figure 3a). There is an in-phase peak at 1.0 PHz and 1.3 PHz. For the 2.4 PHz peak we see an only N[5]; again, this is indicative of participation in another resonance mode. Thus, the electron dynamics does not contribute to the C-N bond elongation or vibration. Although there is no contribution from dynamic electronic effects, the initial gradient discussed above drives the large C-N extension.

To summarise, returning to Figure 5, we have shown that the C-N bond stretching is driven by the gradient, and the C-C and C-OH stretching is driven by the electron dynamics (Figure 8d and Figure 8b).

a

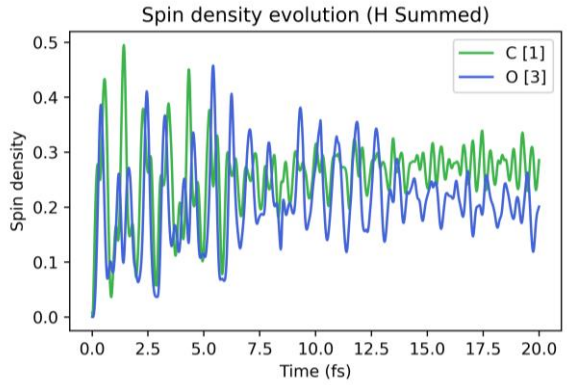

b

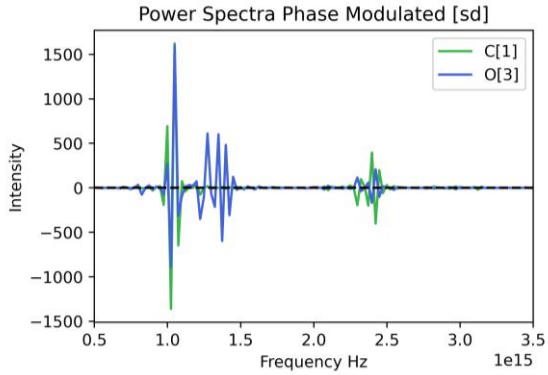

c

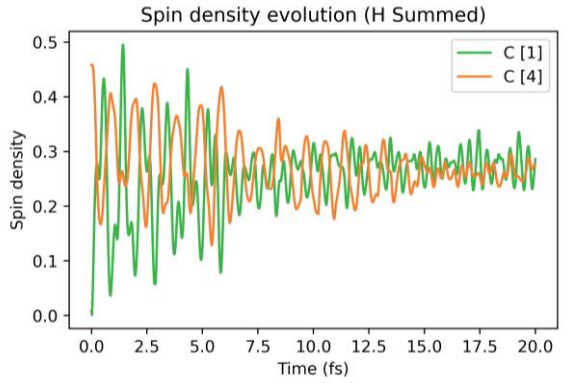

d

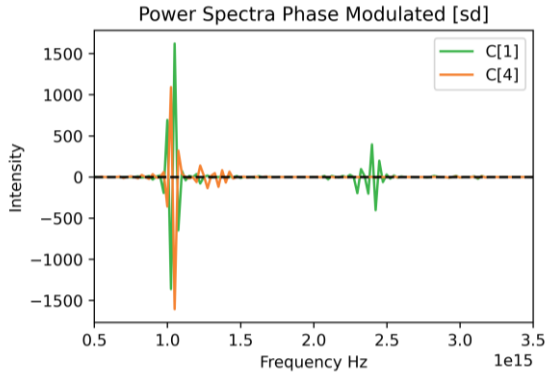

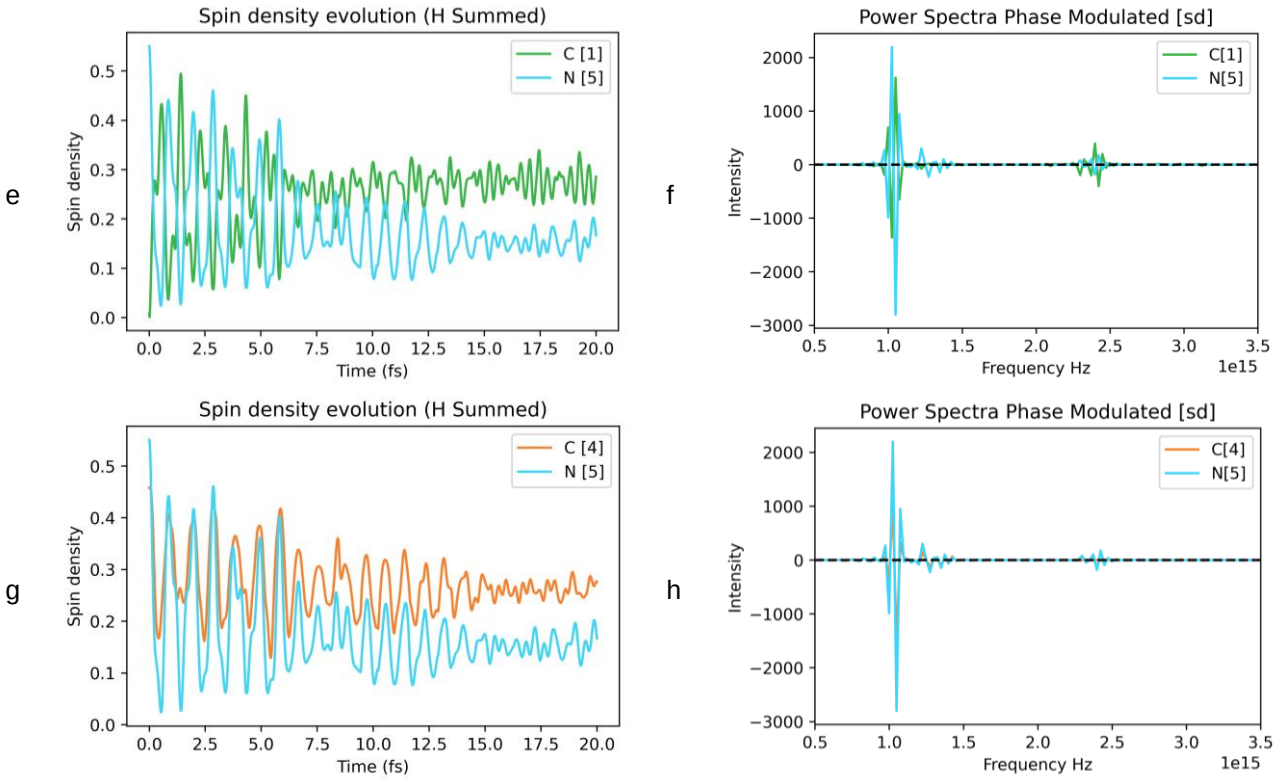

Figure 8 Pair plots of the spin density and its FT spectra for NBO8 (C-N) starting state for (a,b) C[1] ↔ O[3], (c.d) C[1] ↔ C[4], (e,f) C[1] ↔ N[5],(g,h) C[4] ↔ N[5].

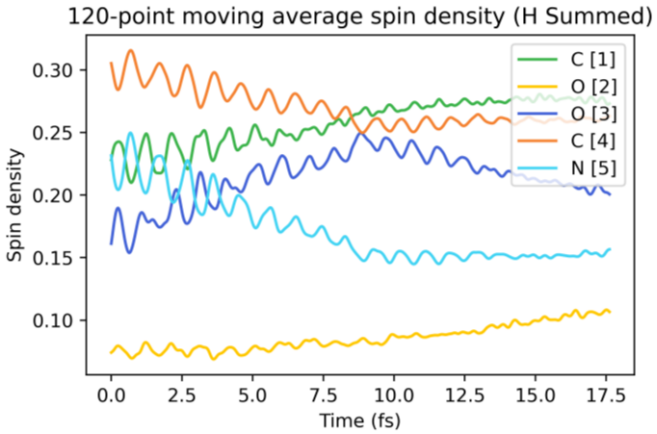

Figure 9 Simple moving average of spin density for the NBO8 starting state. Note the permanent translocation of charge from N[5] and C[4] to O[3], C[1] and O[2] consistent with a charge transfer occurring within the first 8fs.

Lastly, let us consider charge transfer. This can be seen clearly in a moving average plot (Figure 9). One can see the permanent movement of charge from N[5] and C[4] to O[3], C[1] and O[2] (See Scheme 1 middle panel). Note too that the bulk of this transfer occurs within the first 8fs and is then followed by another different charge transfer process. This change is coincident with the turning point in the C=O and C-OH bond lengths seen in Figure 5. We see this effect in the FT spectrum where the same atom pair (e.g. Figure 8f C[1] ↔ N[5]) is involved in several peaks within the 1.0PHz band in Figure 7. The charge transfer seems to affect the short-term electron dynamics by shifting the frequencies of the electron dynamics normal modes.

NBO6 (C-C)

The next set of data to consider is the ionisation from the C-C bond (NBO6). We present the data and a full discussion of this case in SI and briefly summarise the main points here.

The transformation matrix (Figure 2) shows that this localised hole is a superposition dominated by CI_3, CI_5 and CI_6. Through these adiabatic states NBO6 is coupled to NBO8 (C-N), NBO1 (C-OH) and the lone pairs. We therefore expect complex multi-state behaviour.

Although we ionised from the C-C, we observe almost no C-C extension – rather, we see large C-N and C=O bond extensions and a C-OH compression.

The initial gradient is small, so the nuclear evolution is controlled mainly by electron dynamics mechanisms. There is also minimal charge transfer, so we expect charge migration to dominate in this system

The FT spectrum of the electron dynamics normal modes has 3 dominant bands of peaks (at 1.0, 1.3 and 2.3 PHz). And again, we have good alignment of ED-NM characteristic frequencies and adiabatic state gaps (seen in Figure 2) given by Eq 1d:

- Band 1: 1.0 PHz = 4.1 eV corresponds to the adiabatic state CI_5/CI_6 gap of 4.4 eV.
- Band 2: 1.3 PHz = 5.4 eV corresponds to the CI_3/CI_5 gap of 5.9 eV.
- Band 3: 2.3 PHz = 9.5 eV corresponds to the CI_3/CI_6 gap of 10.3 eV

This example highlights the importance of the population of vibrational normal modes: the C[4] ↔C[1] APR ought drive a C-C extension (and indeed we observe excitation of NM8) yet the C[1] ↔ O[2] APR drives excitation of NM19 and this effectively cancels out the C-C extension.

The other interesting feature of the NBO6 simulations is that there is no charge transfer. Consequently, we do not see the damping of the spin density oscillations seen for NBO8 in Figure 8. One might ask when decoherence would begin to occur for NBO6 and whether the long-lived coherence seen in NBO6 is an artifact of the Ehrenfest method. Jenkins et al[27] have shown that two nuclear wavepackets moving on different electronic surfaces leads to similar decoherence of the electron dynamics as the Ehrenfest method used here since GWPs at different coordinates experience surfaces that relate to different adiabatic state mixtures.

Conclusion

In this work we have shown that ionization from a localized orbital (or, equivalently, the population of a specific coherent superposition of adiabatic states) leads to electron dynamics driven nuclear motion. There are 3 mechanisms that control the nuclear dynamics: the initial gradient, charge transfer and charge migration.

The electron dynamics has been characterized through a phase-modulated discrete Fourier transform of the heavy-atom projected spin densities. One can identify bands and characteristic frequencies (electron dynamics normal modes (ED-NM). These are the fundamental modes of the electron dynamics within the system that correspond to the energy gaps of the constituent adiabatic states. Furthermore, this analysis reveals the pairs of out of phase, oscillating atomic spin densities (the atom pair resonances or APR) involved in these electron dynamics modes. Such APR are the basis in which one can express the ED-NM, although the exact combinations are not directly accessible with current theory. These APR provide a simple correlation with the atom-atom nuclear motion. Thus, an active APR should lead to a nuclear distortion between the atoms involved.

Finally, we shall briefly discuss the experimental feasibility of generating such localized hole states. One approach, if only the highest lying outer valence states are of importance in the localised NBO state, is to use the selectivity inherent in short pulse ionisation by an ultraviolet pulse (via a single photon channel) or strong field ionisation (by a strong visible or IR field) that strongly selects a superposition of the outermost valence states. Such superpositions formed by a strong field ionisation process have been observed in a number of high-harmonic based experiments[32] and used to study charge migration in a recent example[33]. An alternative possibility that may access to a wider range of superposition states corresponding to initially localised hole states is to use impulsive X-ray Raman processes mediated by core excited intermediates states to excite localised electronic states as has been proposed and developed by the Mukamel group[34] and recently demonstrated[35] . In such schemes the intermediate resonance enhancement of the Raman process can lead to the selective excitation of atomically localised superposition states. Such an idea should be extendable to creating localised cationic electronic superpositions of the kind studied here, although this has not yet been achieved experimentally to our knowledge.

Supplementary information

The simulation parameters and similar details. A full discussion of NBO6 as well as a brief documentation results for NBO1 and NBO3 starting states are presented in the supplementary information

Acknowledgements

The authors are grateful for financial support from Gaussian, Inc. and the UK Engineering and Physical Science Research Council (grant EP/T006943/1).

All computations were carried out at the Imperial College Research Computing Service (DOI: 10.14469/hpc/2232).

Bibliography

[1] F.I. Vilesov, B.L. Kurbatov, and A.N. Terenin, Soviet Physics Doklady **6**, 490 (1961).
[2] W.C. Price, in *Advances in Atomic and Molecular Physics* (Elsevier, 1974), pp. 131–171.
[3] T. Koopmans, Physica **1**, 104 (1934).
[4] I.C.D. Merritt, D. Jacquemin, and M. Vacher, J. Phys. Chem. Lett. **12**, 8404 (2021).
[5] A.S. Johnson, D.R. Austin, D.A. Wood, C. Brahms, A. Gregory, K.B. Holzner, S. Jarosch, E.W. Larsen, S. Parker, C.S. Strüber, P. Ye, J.W.G. Tisch, and J.P. Marangos, Sci. Adv. **4**, eaar3761 (2018).
[6] D. Popmintchev, B.R. Galloway, M.-C. Chen, F. Dollar, C.A. Mancuso, A. Hankla, L. Miaja-Avila, G. O'Neil, J.M. Shaw, G. Fan, S. Ališauskas, G. Andriukaitis, T. Balčiunas, O.D. Mücke, A. Pugzlys, A. Baltuška, H.C. Kapteyn, T. Popmintchev, and M.M. Murnane, Phys. Rev. Lett. **120**, 093002 (2018).
[7] J. Duris, S. Li, T. Driver, E.G. Champenois, J.P. MacArthur, A.A. Lutman, Z. Zhang, P. Rosenberger, J.W. Aldrich, R. Coffee, G. Coslovich, F.-J. Decker, J.M. Glownia, G. Hartmann, W. Helml, A. Kamalov, J. Knurr, J. Krzywinski, M.-F. Lin, J.P. Marangos, M. Nantel, A. Natan, J.T. O'Neal, N. Shivaram, P. Walter, A.L. Wang,

J.J. Welch, T.J.A. Wolf, J.Z. Xu, M.F. Kling, P.H. Bucksbaum, A. Zholents, Z. Huang, J.P. Cryan, and A. Marinelli, Nat. Photonics **14**, 30 (2020).
[8] F. Calegari, D. Ayuso, A. Trabattoni, L. Belshaw, S. De Camillis, S. Anumula, F. Frassetto, L. Poletto, A. Palacios, P. Decleva, J.B. Greenwood, F. Martín, and M. Nisoli, Science **346**, 336 (2014).
[9] B. Cooper, P. Kolorenč, L.J. Frasinski, V. Averbukh, and J.P. Marangos, Faraday Discuss. **171**, 93 (2014).
[10] T. Barillot, O. Alexander, B. Cooper, T. Driver, D. Garratt, S. Li, A. Al Haddad, A. Sanchez-Gonzalez, M. Agåker, C. Arrell, M.J. Bearpark, N. Berrah, C. Bostedt, J. Bozek, C. Brahms, P.H. Bucksbaum, A. Clark, G. Doumy, R. Feifel, L.J. Frasinski, S. Jarosch, A.S. Johnson, L. Kjellsson, P. Kolorenč, Y. Kumagai, E.W. Larsen, P. Matia-Hernando, M. Robb, J.-E. Rubensson, M. Ruberti, C. Sathe, R.J. Squibb, A. Tan, J.W.G. Tisch, M. Vacher, D.J. Walke, T.J.A. Wolf, D. Wood, V. Zhaunerchyk, P. Walter, T. Osipov, A. Marinelli, T.J. Maxwell, R. Coffee, A.A. Lutman, V. Averbukh, K. Ueda, J.P. Cryan, and J.P. Marangos, Phys. Rev. X **11**, 031048 (2021).
[11] M. Amarouche, F.X. Gadea, and J. Durup, 13 (n.d.).
[12] D. Mendive-Tapia, M. Vacher, M.J. Bearpark, and M.A. Robb, The Journal of Chemical Physics **139**, 044110 (2013).
[13] T. Tran, G.A. Worth, and M.A. Robb, Commun Chem **4**, 48 (2021).
[14] F. Weinhold and C.R. Landis, Chem. Educ. Res. Pract. **2**, 91 (2001).
[15] I. Polyak, A.J. Jenkins, M. Vacher, M.E.F. Bouduban, M.J. Bearpark, and M.A. Robb, Molecular Physics **116**, 2474 (2018).
[16] D. Schwickert, M. Ruberti, K. Baev, I. Baev, M. Braune, L. Bocklage, K. Czwalinna, S. Deinert, S. Düsterer, A. Hans, C. Haunhorst, M. Kuhlmann, S. Palutke, J. Rönsch-Schulenburg, P. Schmidt, S. Toleikis, M. Martins, A. Knie, D. Kip, V. Averbukh, and T. Laarmann, Arxiv 53 (2021).
[17] A.I. Kuleff, J. Breidbach, and L.S. Cederbaum, The Journal of Chemical Physics **123**, 044111 (2005).
[18] J. Delgado, M. Lara-Astiaso, J. González-Vázquez, P. Decleva, A. Palacios, and F. Martín, Faraday Discuss. 10.1039.D0FD00121J (2021).
[19] M. Lara-Astiaso, D. Ayuso, I. Tavernelli, P. Decleva, A. Palacios, and F. Martín, Faraday Discuss. **194**, 41 (2016).
[20] M. Lara-Astiaso, A. Palacios, P. Decleva, I. Tavernelli, and F. Martín, Chemical Physics Letters **683**, 357 (2017).
[21] H.J. Wörner, C.A. Arrell, N. Banerji, A. Cannizzo, M. Chergui, A.K. Das, P. Hamm, U. Keller, P.M. Kraus, E. Liberatore, P. Lopez-Tarifa, M. Lucchini, M. Meuwly, C. Milne, J.-E. Moser, U. Rothlisberger, G. Smolentsev, J. Teuscher, J.A. van Bokhoven, and O. Wenger, Structural Dynamics **4**, 061508 (2017).
[22] L.S. Cederbaum and J. Zobeley, Chemical Physics Letters **307**, 205 (1999).
[23] I. Polyak, M.J. Bearpark, and M.A. Robb, Int J Quantum Chem **118**, e25559 (2018).
[24] W. Kauzmann, *Quantum Chemistry: An Introduction.* (Elsevier Science, Saint Louis, 2013).
[25] J.W. Cooley and J.W. Tukey, 5 (n.d.).
[26] C.R. Harris, K.J. Millman, S.J. van der Walt, R. Gommers, P. Virtanen, D. Cournapeau, E. Wieser, J. Taylor, S. Berg, N.J. Smith, R. Kern, M. Picus, S. Hoyer, M.H. van Kerkwijk, M. Brett, A. Haldane, J.F. del Río, M. Wiebe, P. Peterson, P. Gérard-Marchant, K. Sheppard, T. Reddy, W. Weckesser, H. Abbasi, C. Gohlke, and T.E. Oliphant, Nature **585**, 357 (2020).
[27] A.J. Jenkins, K.E. Spinlove, M. Vacher, G.A. Worth, and M.A. Robb, The Journal of Chemical Physics **149**, 094108 (2018).
[28] G.W. Richings, I. Polyak, K.E. Spinlove, G.A. Worth, I. Burghardt, and B. Lasorne, International Reviews in Physical Chemistry **34**, 269 (2015).
[29] M. Vacher, D. Mendive-Tapia, M.J. Bearpark, and M.A. Robb, Theor Chem Acc **133**, 1505 (2014).
[30] M.J. Frisch, G.W. Trucks, H.B. Schlegel, G.E. Scuseria, M.A. Robb, J.R. Cheeseman, G. Scalmani, V. Barone, G.A. Petersson, H. Nakatsuji, X. Li, M. Caricato, A.V. Marenich, J. Bloino, B.G. Janesko, R. Gomperts, B. Mennucci, H.P. Hratchian, J.V. Ortiz, A.F. Izmaylov, J.L. Sonnenberg, Williams, F. Ding, F. Lipparini, F. Egidi, J. Goings, B. Peng, A. Petrone, T. Henderson, D. Ranasinghe, V.G. Zakrzewski, J. Gao, N. Rega, G. Zheng, W. Liang, M. Hada, M. Ehara, K. Toyota, R. Fukuda, J. Hasegawa, M. Ishida, T. Nakajima, Y. Honda, O. Kitao, H. Nakai, T. Vreven, K. Throssell, J.A. Montgomery Jr., J.E. Peralta, F. Ogliaro, M.J. Bearpark, J.J. Heyd, E.N. Brothers, K.N. Kudin, V.N. Staroverov, T.A. Keith, R. Kobayashi, J. Normand, K. Raghavachari, A.P. Rendell, J.C. Burant, S.S. Iyengar, J. Tomasi, M. Cossi, J.M. Millam, M. Klene, C. Adamo, R. Cammi, J.W. Ochterski, R.L. Martin, K. Morokuma, O. Farkas, J.B. Foresman, and D.J. Fox, *Gaussian Development Version Rev. J05* (Gaussian Inc, Wallingford, CT, 2019).
[31] G.A. Worth, K. Giri, G. Richings, I. Burghardt, M. Beck, A. Jäckle, and H. Meyer, *The QUANTICS Package* (University of Birmingham, 2015).
[32] O. Smirnova, Y. Mairesse, S. Patchkovskii, N. Dudovich, D. Villeneuve, P. Corkum, and M.Yu. Ivanov, Nature **460**, 972 (2009).

[33] P.M. Kraus, B. Mignolet, D. Baykusheva, A. Rupenyan, L. Horný, E.F. Penka, G. Grassi, O.I. Tolstikhin, J. Schneider, F. Jensen, L.B. Madsen, A.D. Bandrauk, F. Remacle, and H.J. Wörner, Science **350**, 790 (2015).
[34] S. Tanaka and S. Mukamel, Phys. Rev. Lett. **89**, 043001 (2002).
[35] J.T. O'Neal, E.G. Champenois, S. Oberli, R. Obaid, A. Al-Haddad, J. Barnard, N. Berrah, R. Coffee, J. Duris, G. Galinis, D. Garratt, J.M. Glownia, D. Haxton, P. Ho, S. Li, X. Li, J. MacArthur, J.P. Marangos, A. Natan, N. Shivaram, D.S. Slaughter, P. Walter, S. Wandel, L. Young, C. Bostedt, P.H. Bucksbaum, A. Picón, A. Marinelli, and J.P. Cryan, Phys. Rev. Lett. **125**, 073203 (2020).

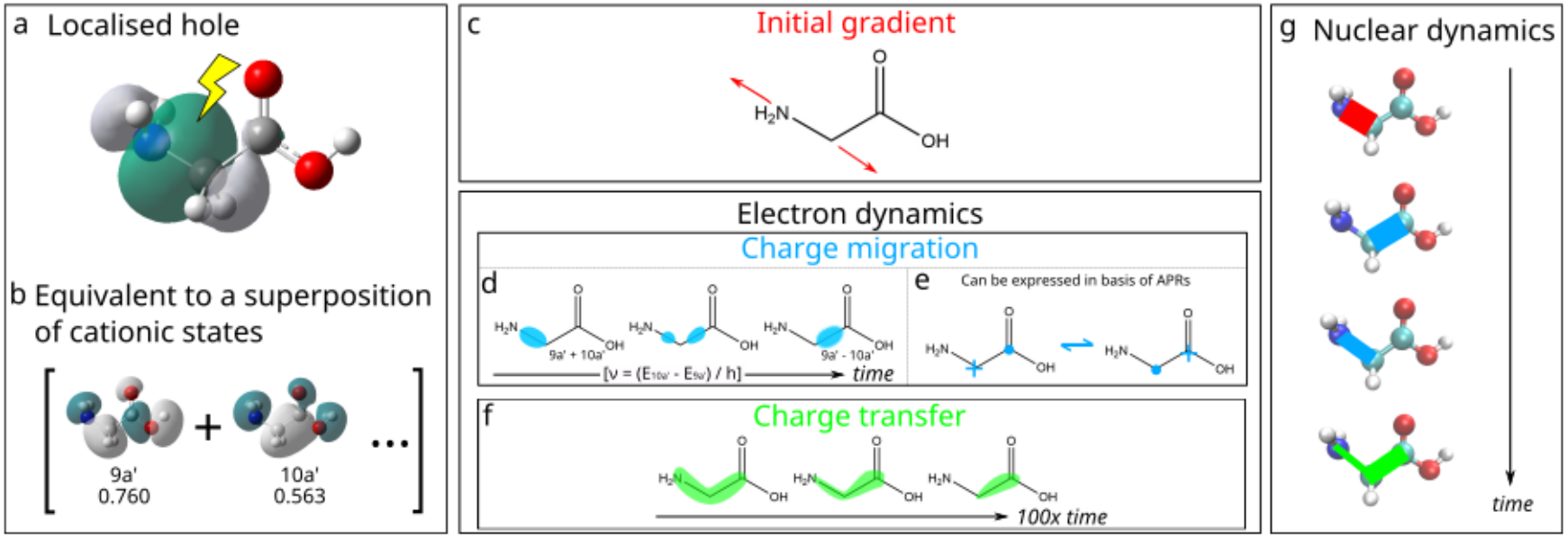

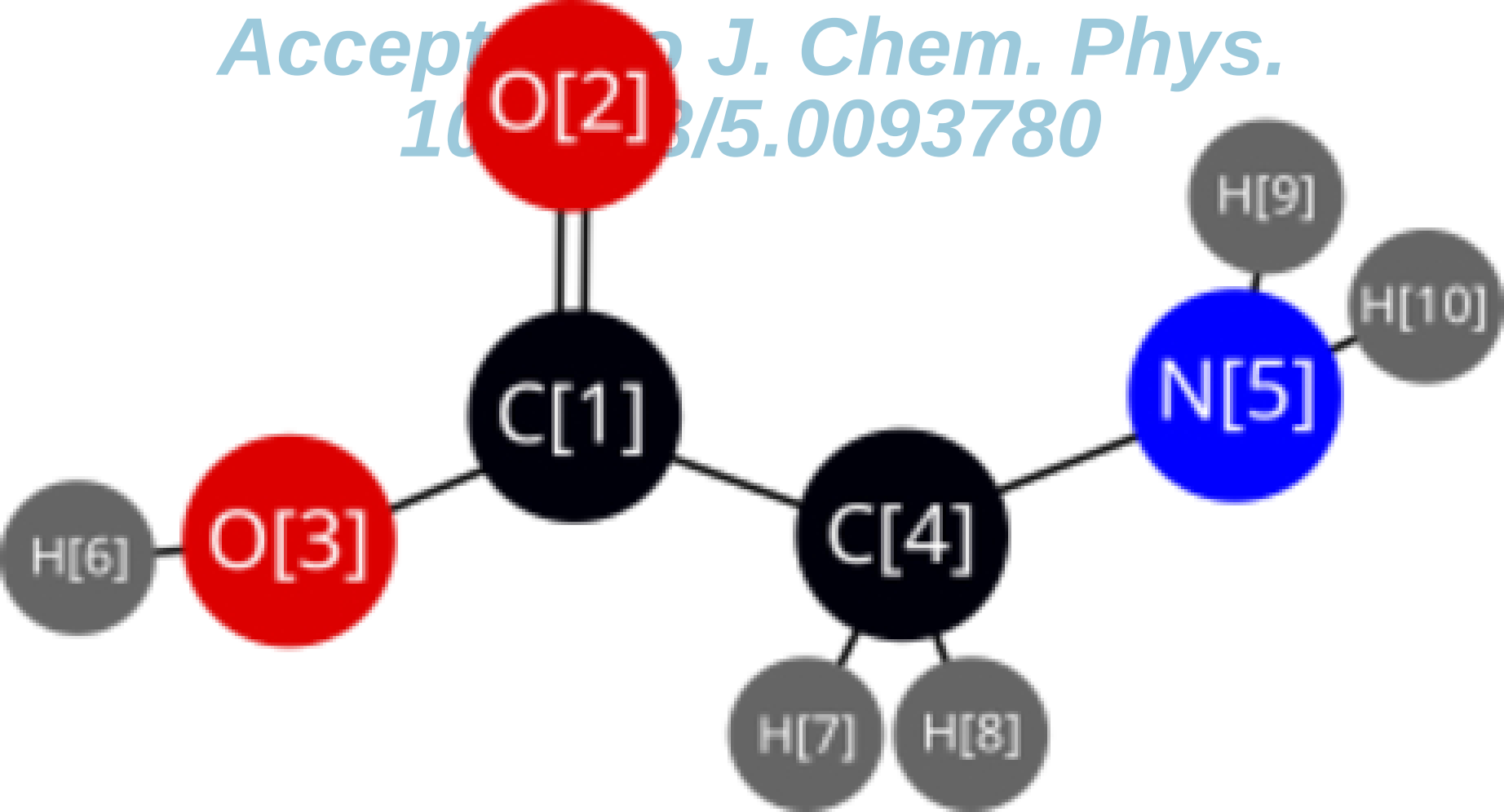

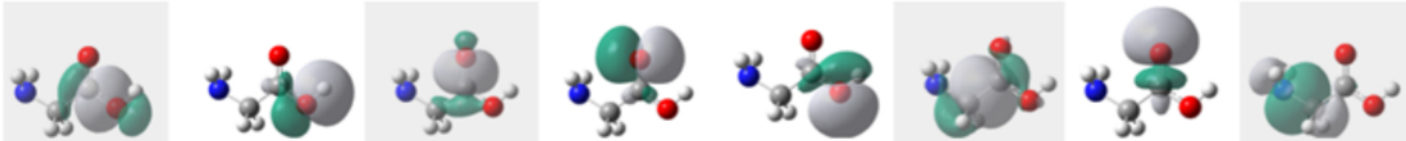

	NBO_1	NBO_2	NBO_3	NBO_4	NBO_5	NBO_6	NBO_7	NBO_8	Energy [eV]	Symmetry
CI_1	0.2216298	0.0120480	0.0019619	0.9201116	0.2175083	-0.2308964	0.0120945	-0.0579364	0.0	15a′
CI_2	0.1348270	-0.3551293	0.3891814	-0.0816426	0.5733370	0.3279627	0.4995947	0.1082014	3.9193	13a′
CI_3	0.5371606	0.3856132	0.0778165	-0.3426892	0.2377957	-0.5234704	0.1471610	-0.2950343	6.7584	11a′/12a′
CI_4	-0.0111017	0.4511562	0.3534264	0.1593372	-0.5368070	0.1660805	0.5735594	0.0363504	7.3375	12a′/11a′
CI_5	0.3755901	0.4853876	-0.0752225	0.0017301	0.1888725	0.4125462	-0.3070593	0.5634865	12.6553	10a′
CI_6	-0.0729007	-0.1761335	-0.0215735	-0.0599991	-0.0820381	-0.5755538	0.2087885	0.7602711	17.0542	9a′
CI_7	0.5093371	-0.4130587	0.5145817	-0.0143565	-0.4126581	0.0007593	-0.3662382	0.0232379	30.5127	7a′
CI_8	-0.4880885	0.2902704	0.6683189	0.0097930	0.2580243	-0.1899113	-0.3572446	0.0223633	33.9105	6a′

NBO_N is CSF where NBO-N is singly occupied … i.e. hole location

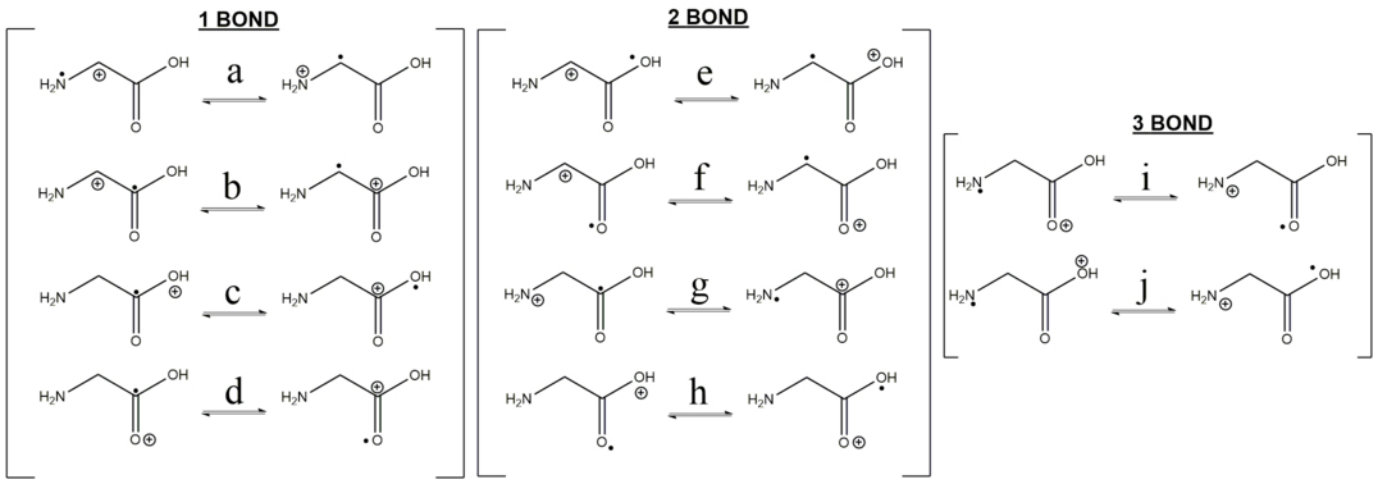
1 BOND
2 BOND
3 BOND
a
b
c
d
e
f
g
h
i
j

Accepted to J. Chem. Phys. 10.1063/5.0093780

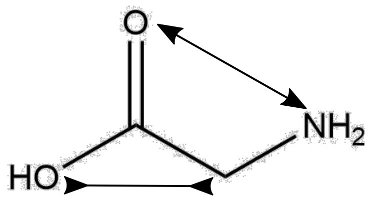

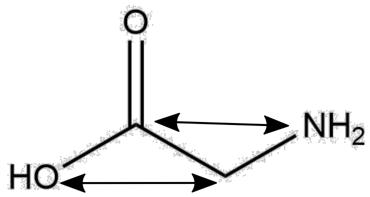

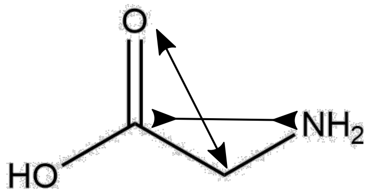

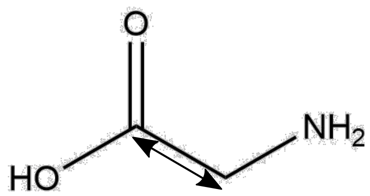

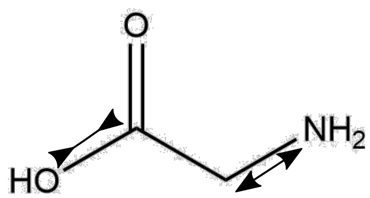

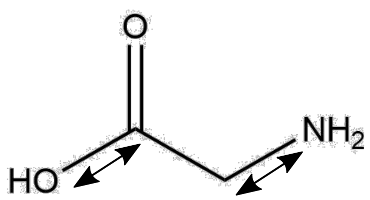

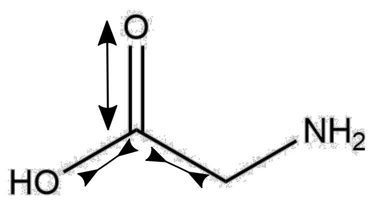

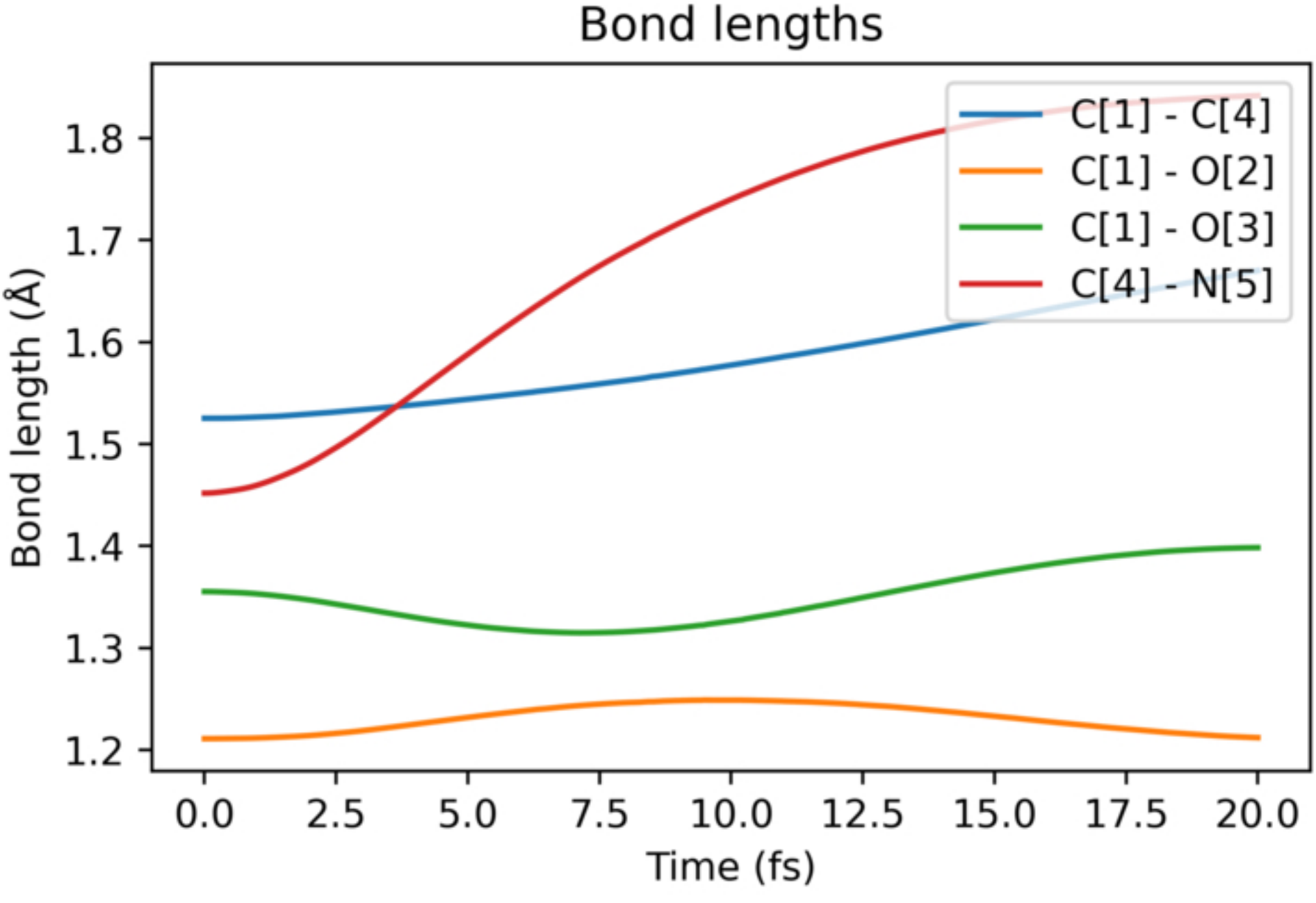
Bond lengths
C[1] - C[4]
C[1] - O[2]
C[1] - O[3]
C[4] - N[5]
Bond length (Å)
1.8
1.7
1.6
1.5
1.4
1.3
1.2
0.0
2.5
5.0
7.5
10.0
12.5
15.0
17.5
20.0
Time (fs)

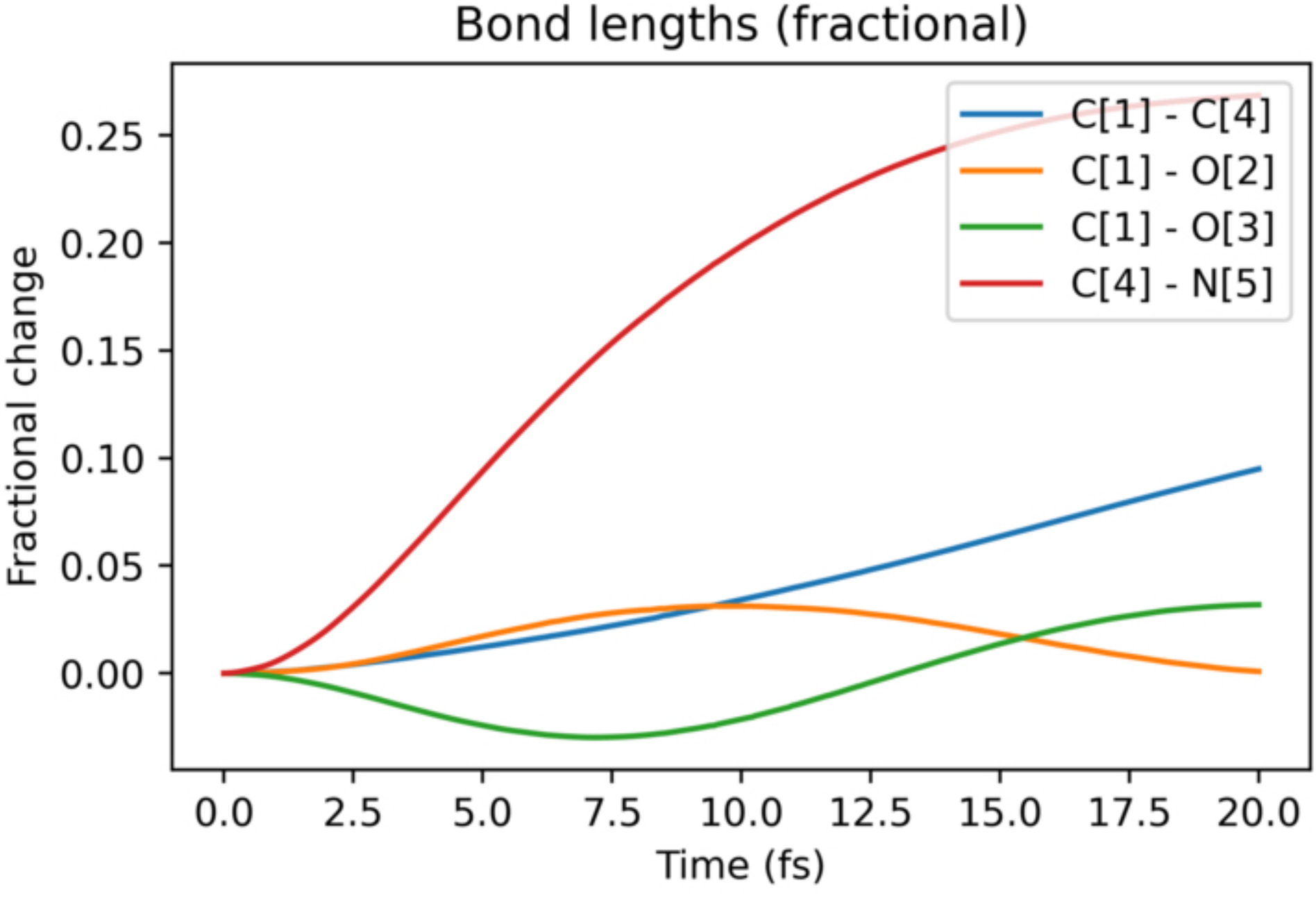
Bond lengths (fractional)
C[1] - C[4]
C[1] - O[2]
C[1] - O[3]
C[4] - N[5]
Fractional change
0.25
0.20
0.15
0.10
0.05
0.00
0.0
2.5
5.0
7.5
10.0
12.5
15.0
17.5
20.0
Time (fs)

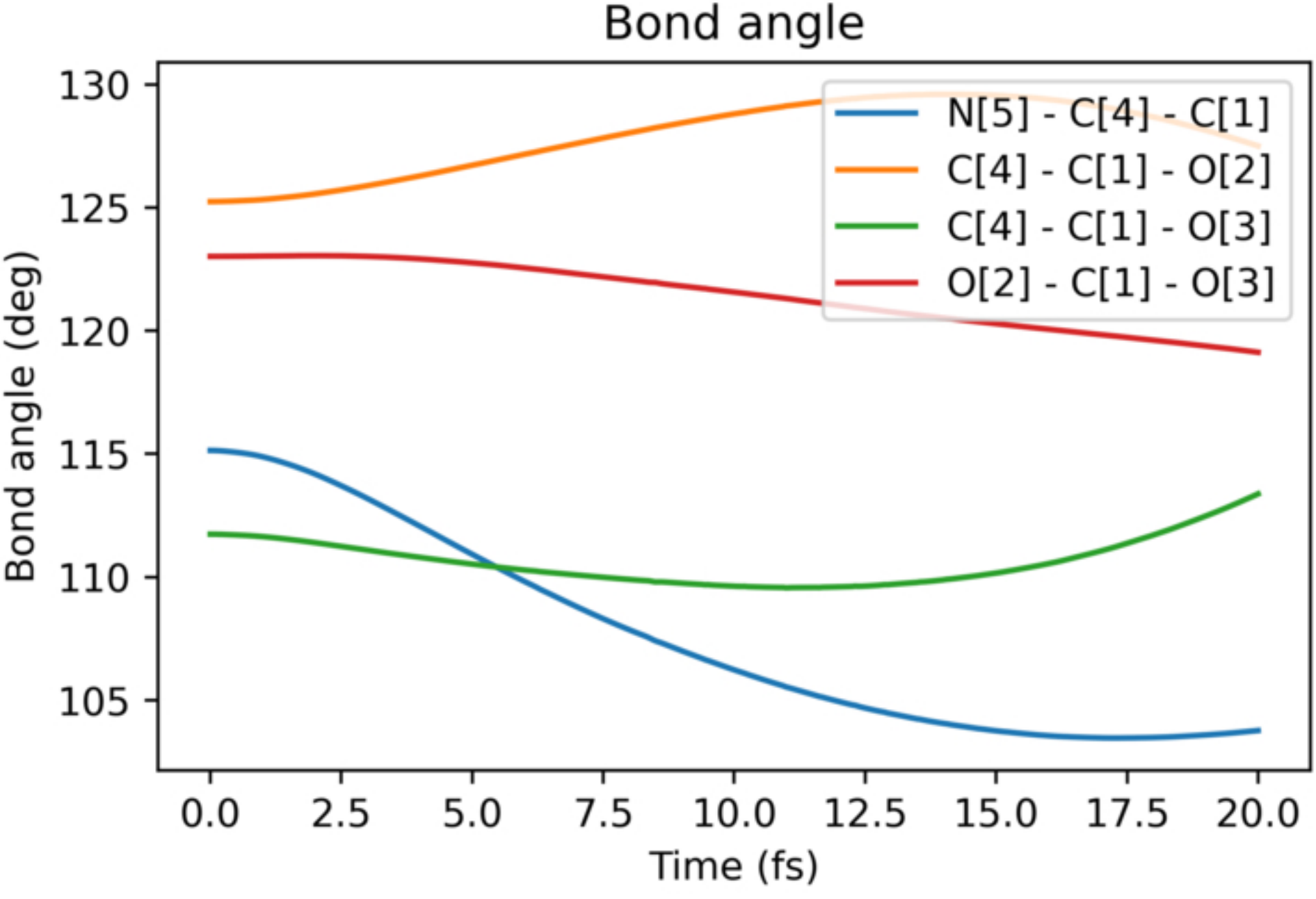
Bond angle
130
125
120
115
110
105
Bond angle (deg)
0.0
2.5
5.0
7.5
10.0
12.5
15.0
17.5
20.0
Time (fs)
N[5] - C[4] - C[1]
C[4] - C[1] - O[2]
C[4] - C[1] - O[3]
O[2] - C[1] - O[3]

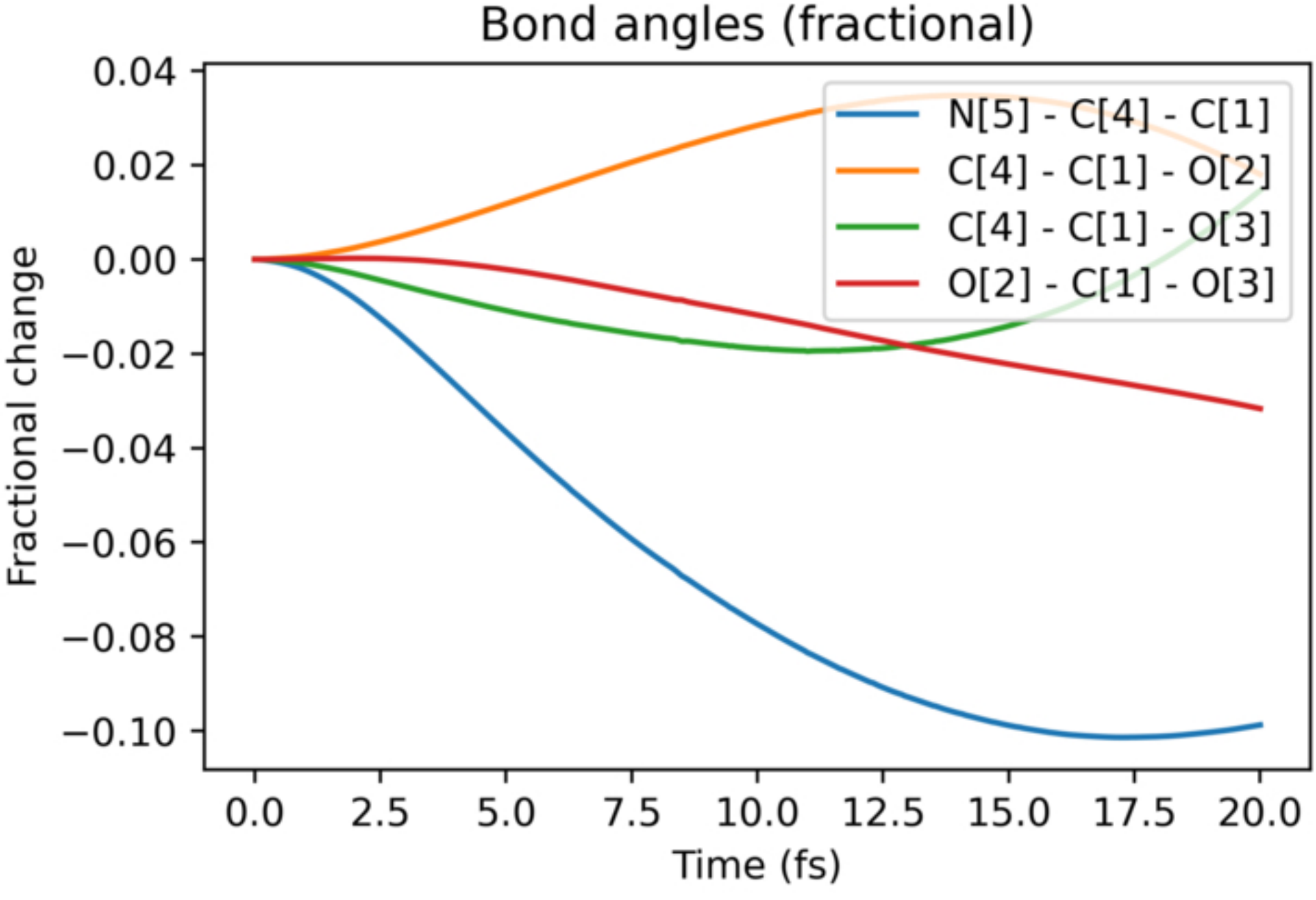
Bond angles (fractional)
N[5] - C[4] - C[1]
C[4] - C[1] - O[2]
C[4] - C[1] - O[3]
O[2] - C[1] - O[3]
Fractional change
0.04
0.02
0.00
−0.02
−0.04
−0.06
−0.08
−0.10
0.0
2.5
5.0
7.5
10.0
12.5
15.0
17.5
20.0
Time (fs)

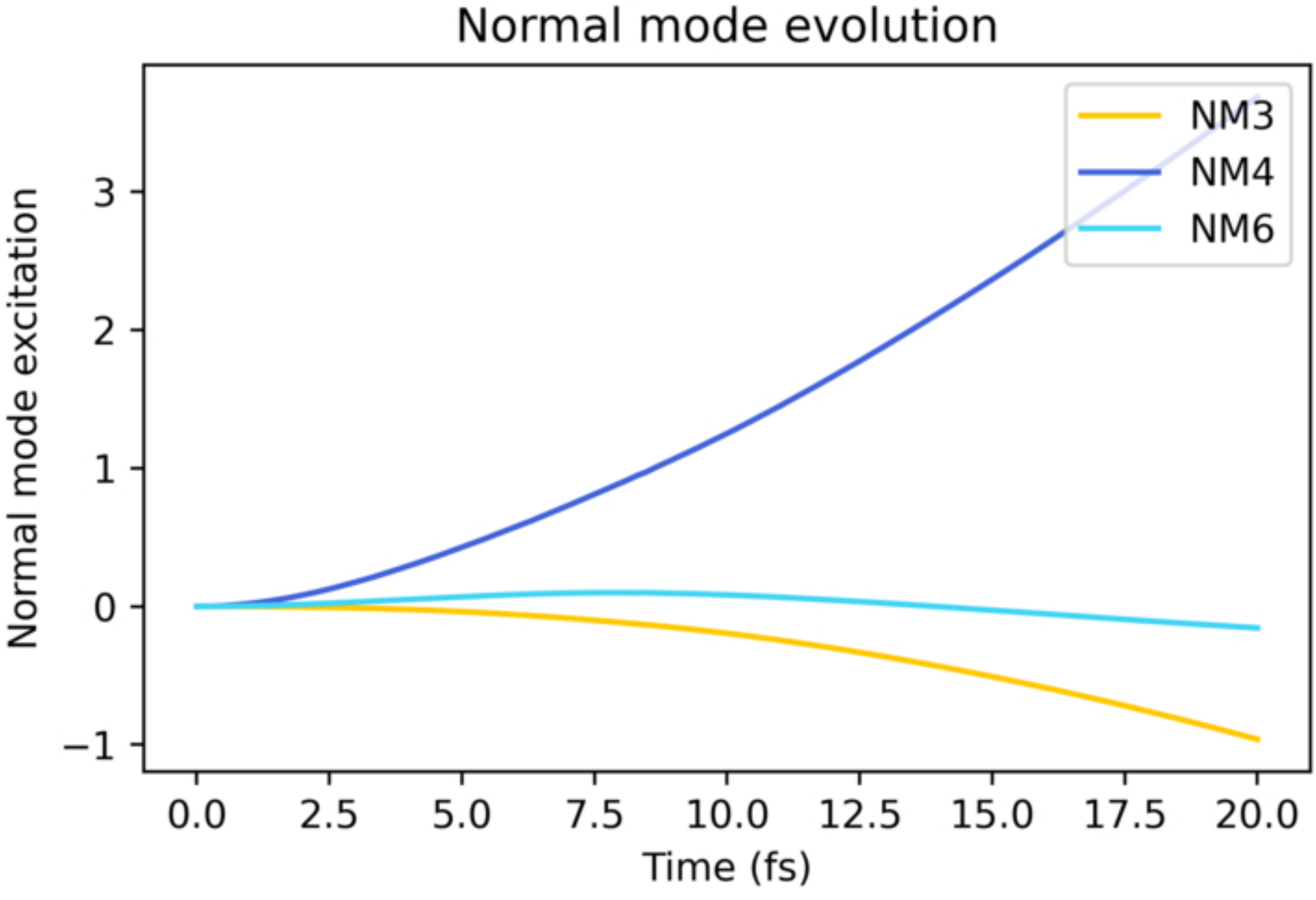
Normal mode evolution
NM3
NM4
NM6
Normal mode excitation
3
2
1
0
−1
0.0
2.5
5.0
7.5
10.0
12.5
15.0
17.5
20.0
Time (fs)

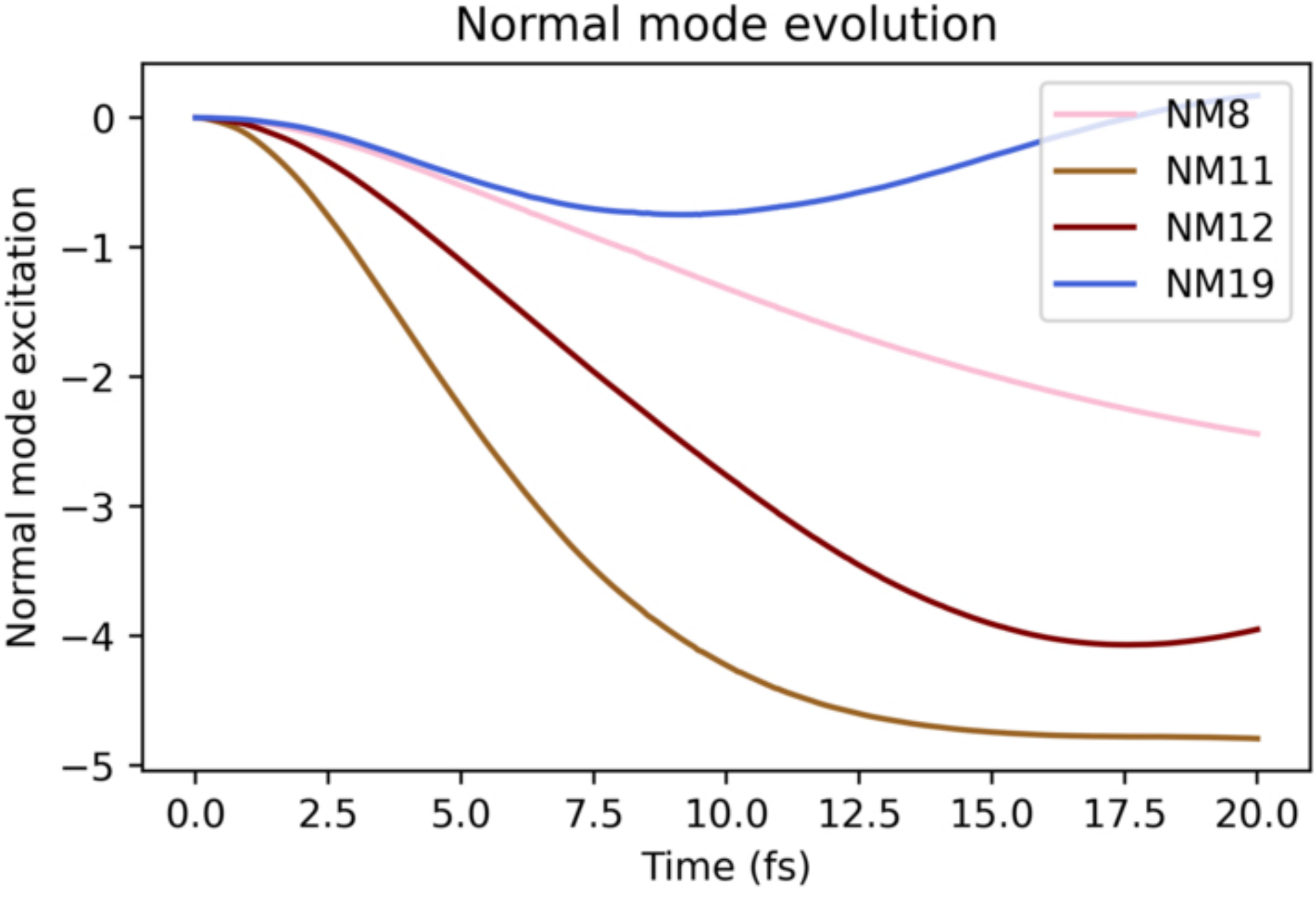
Normal mode evolution
NM8
NM11
NM12
NM19
Normal mode excitation
0
−1
−2
−3
−4
−5
0.0
2.5
5.0
7.5
10.0
12.5
15.0
17.5
20.0
Time (fs)

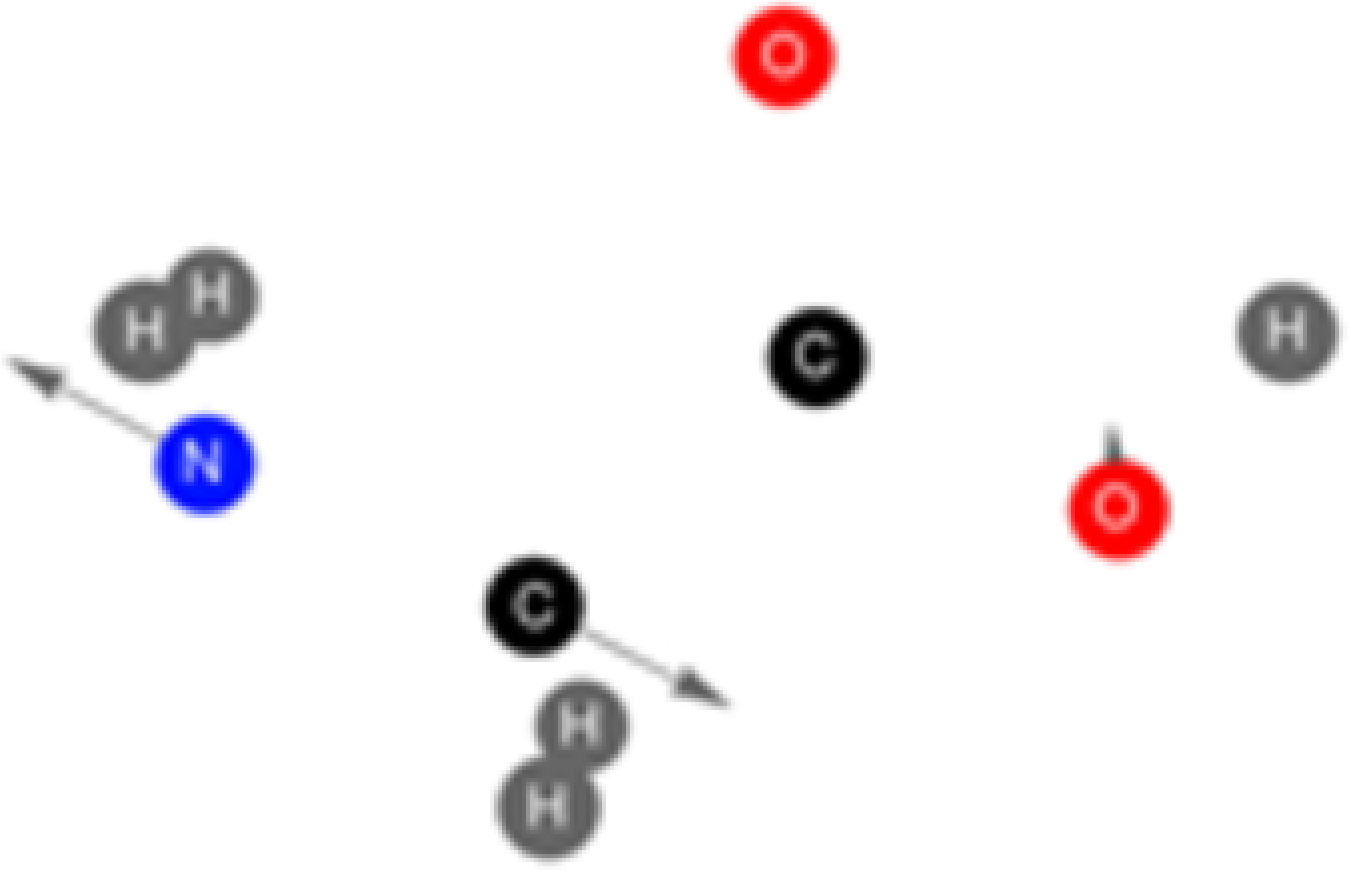
O
H
H
C
H
N
O
C
H
H

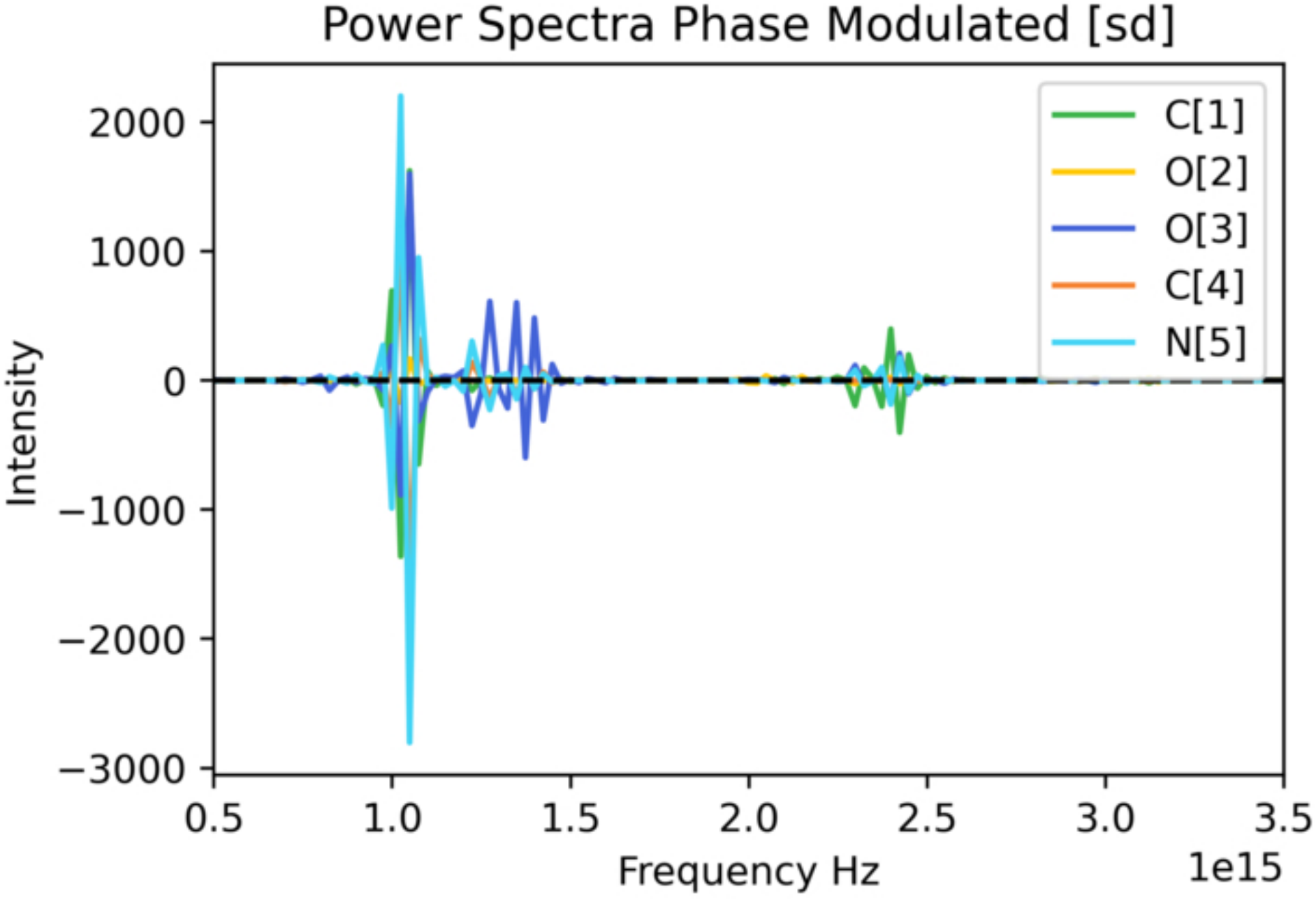
Power Spectra Phase Modulated [sd]
C[1]
O[2]
O[3]
C[4]
N[5]
2000
1000
0
−1000
−2000
−3000
Intensity
0.5
1.0
1.5
2.0
2.5
3.0
3.5
Frequency Hz
1e15

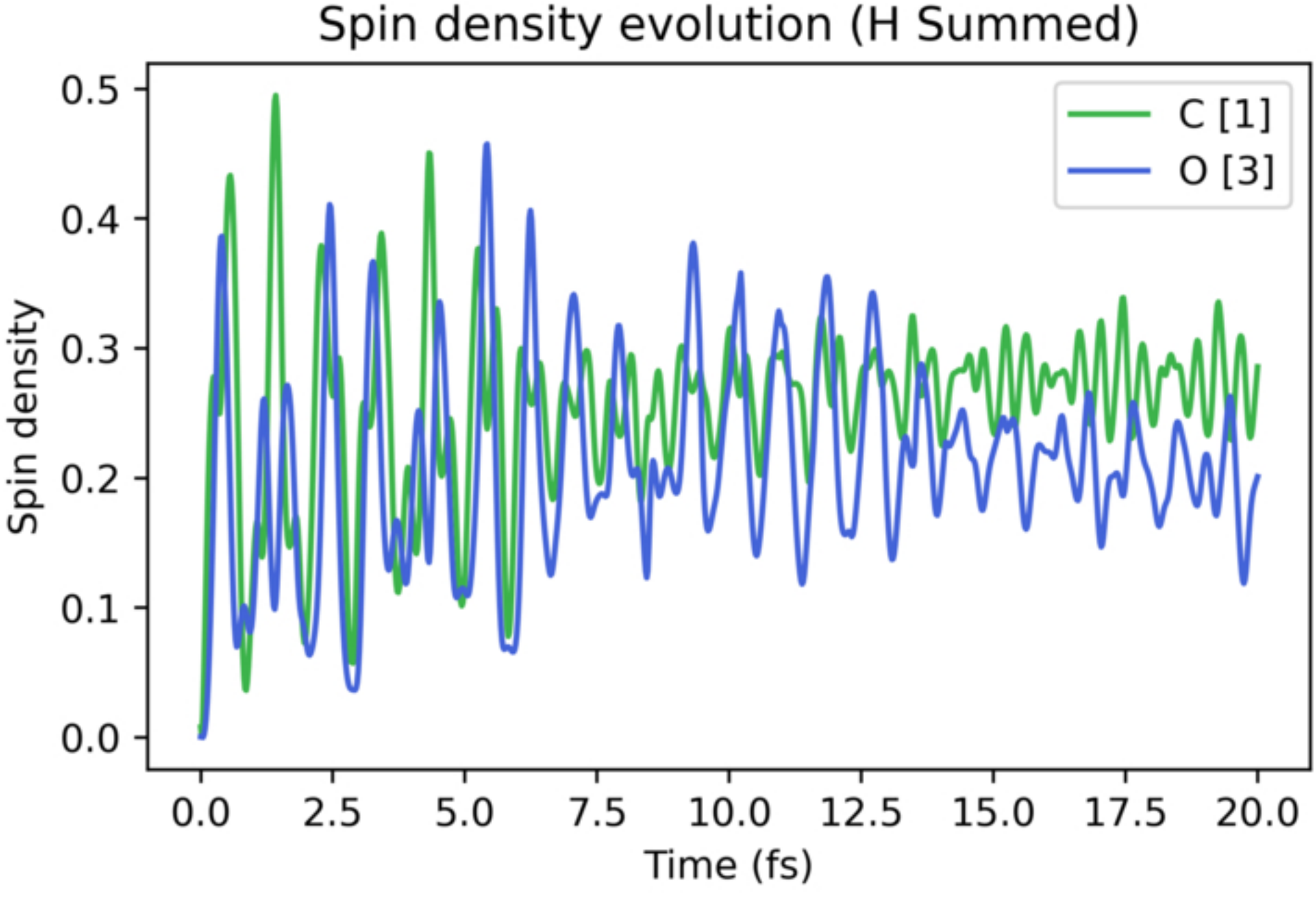
Spin density evolution (H Summed)
C [1]
O [3]
Spin density
Time (fs)
0.0
0.1
0.2
0.3
0.4
0.5
0.0
2.5
5.0
7.5
10.0
12.5
15.0
17.5
20.0

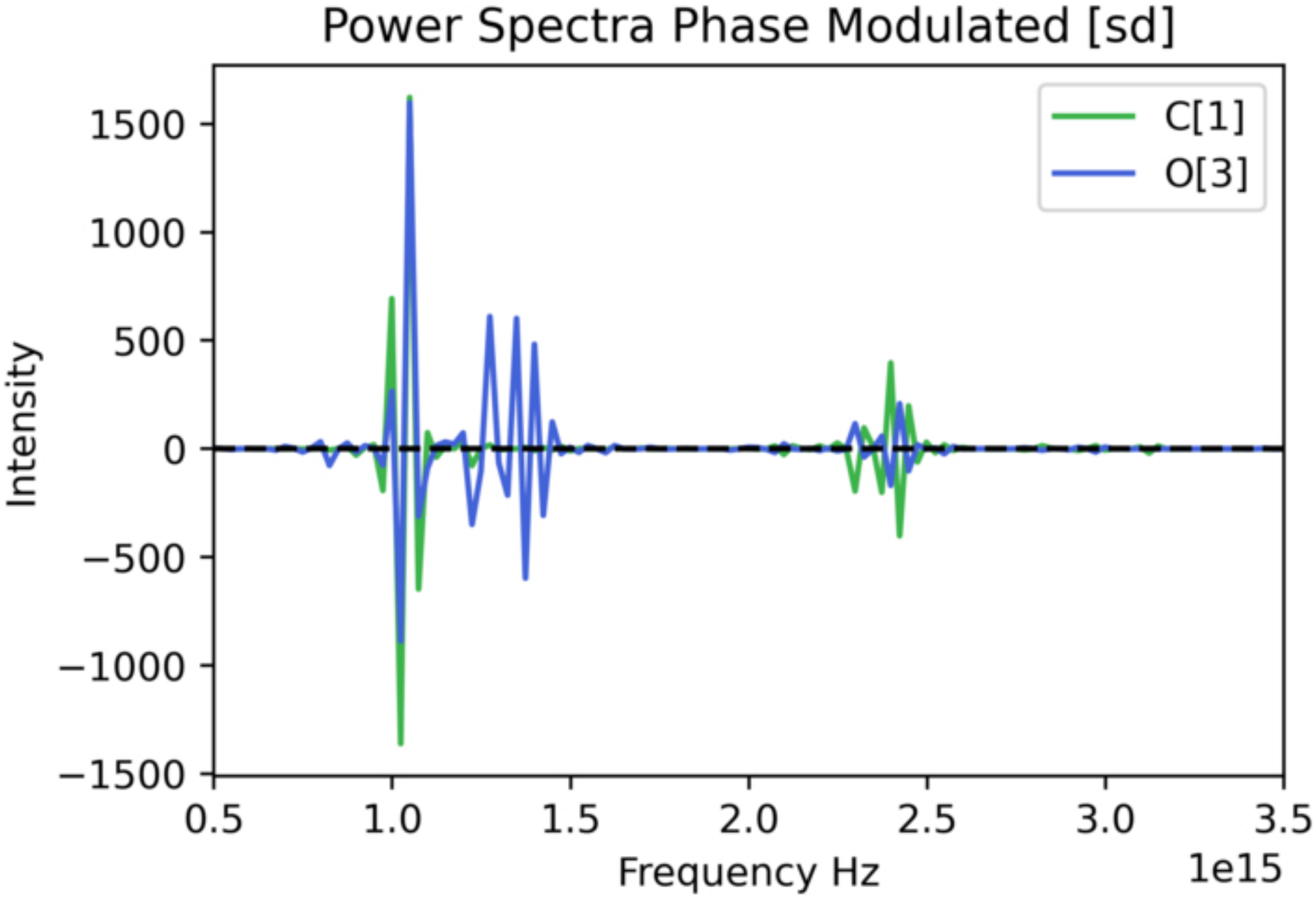
Power Spectra Phase Modulated [sd]
C[1]
O[3]
1500
1000
500
0
−500
−1000
−1500
Intensity
0.5
1.0
1.5
2.0
2.5
3.0
3.5
Frequency Hz
1e15

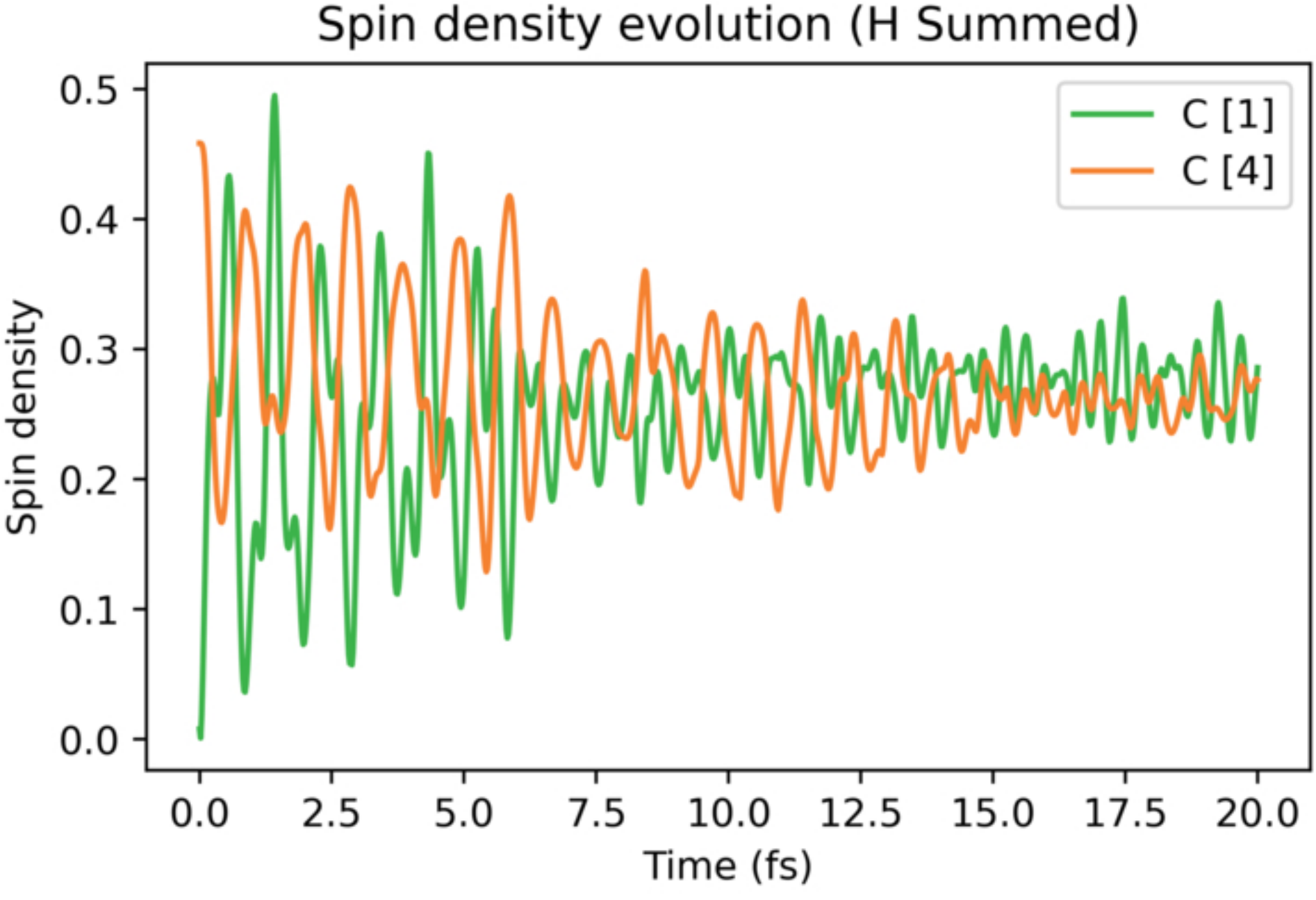
Spin density evolution (H Summed)
C [1]
C [4]
Spin density
0.0
0.1
0.2
0.3
0.4
0.5
0.0
2.5
5.0
7.5
10.0
12.5
15.0
17.5
20.0
Time (fs)

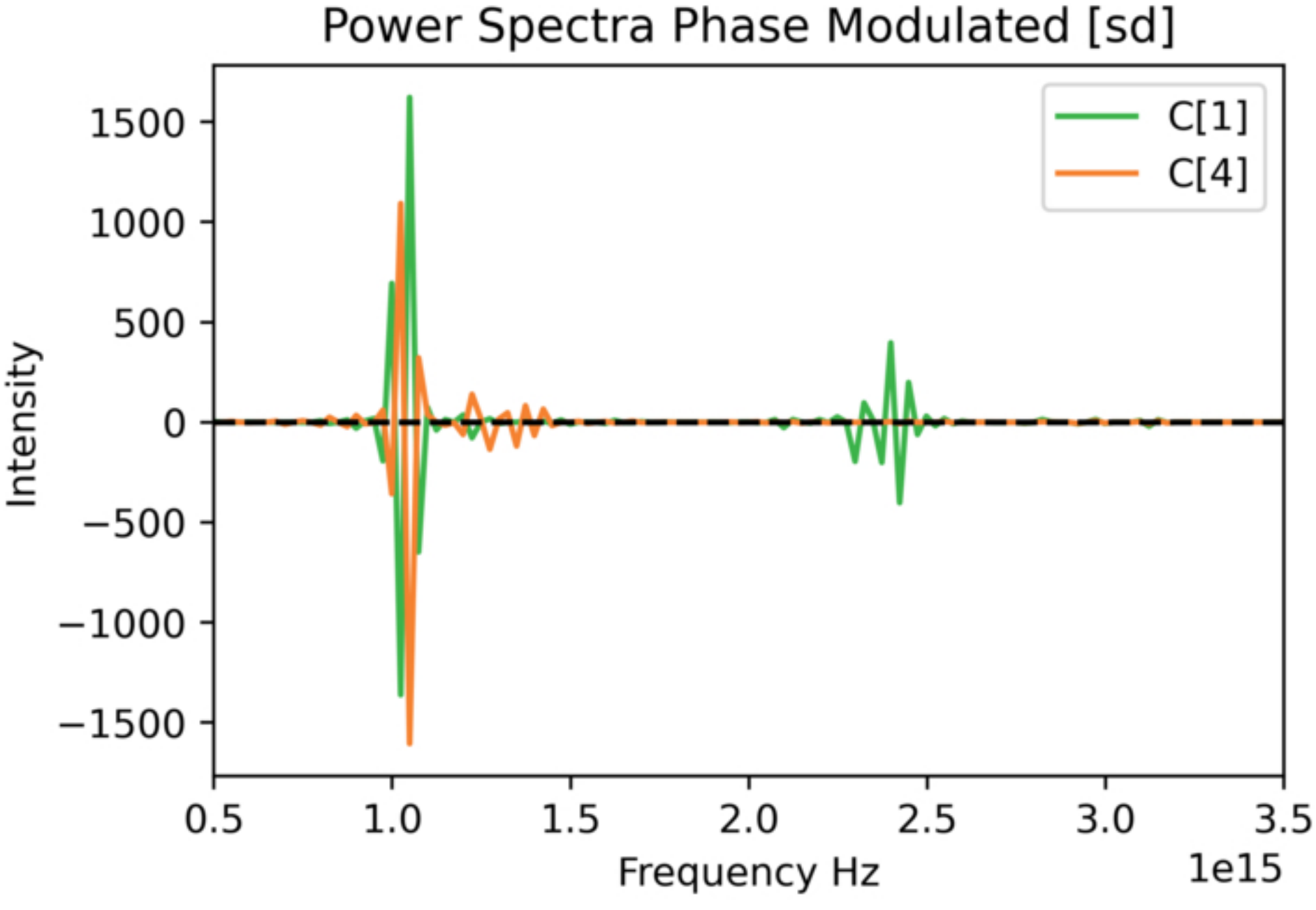
Power Spectra Phase Modulated [sd]
C[1]
C[4]
1500
1000
500
0
−500
−1000
−1500
Intensity
0.5
1.0
1.5
2.0
2.5
3.0
3.5
Frequency Hz
1e15

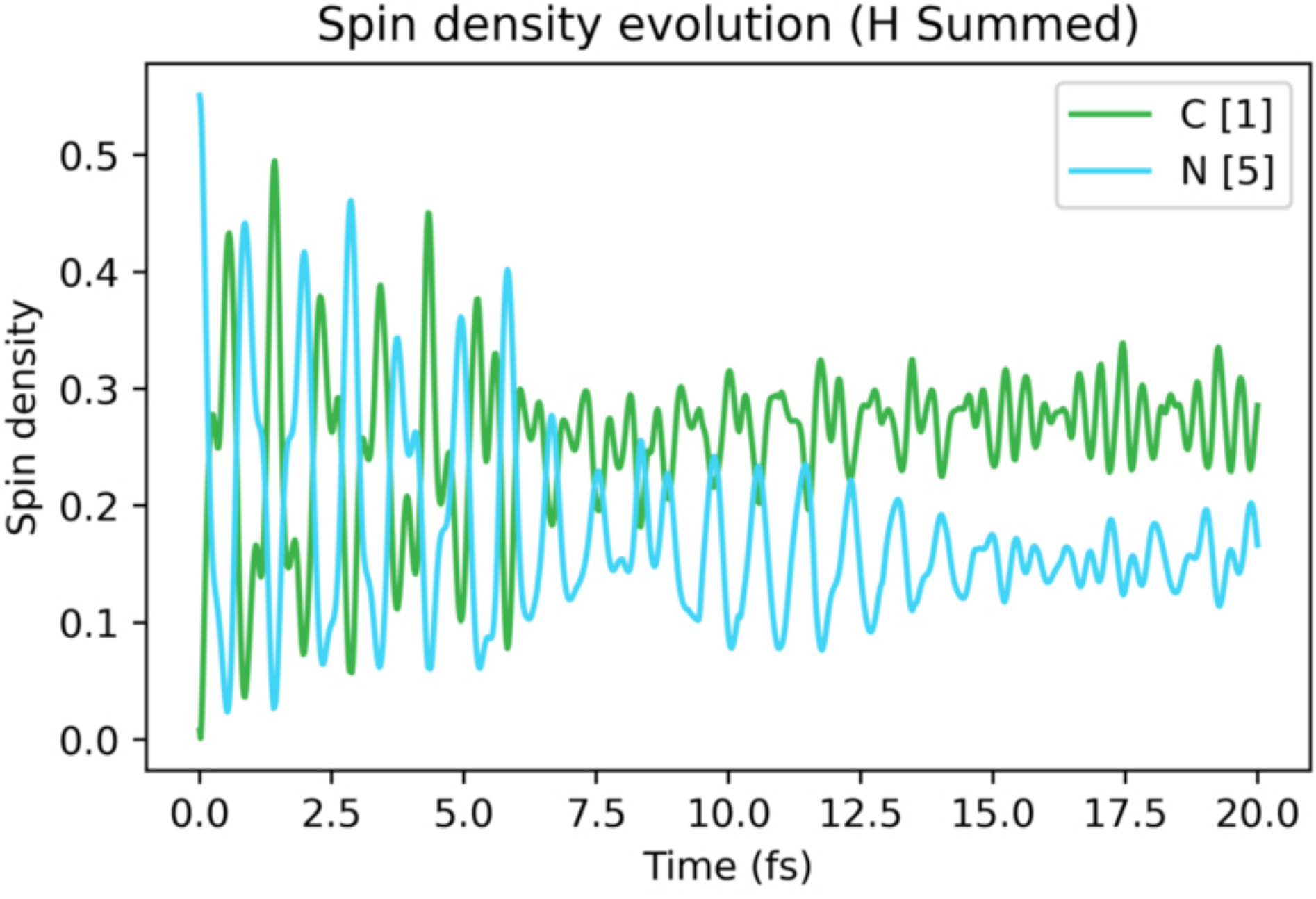
Spin density evolution (H Summed)
C [1]
N [5]
Spin density
0.0
0.1
0.2
0.3
0.4
0.5
0.0
2.5
5.0
7.5
10.0
12.5
15.0
17.5
20.0
Time (fs)

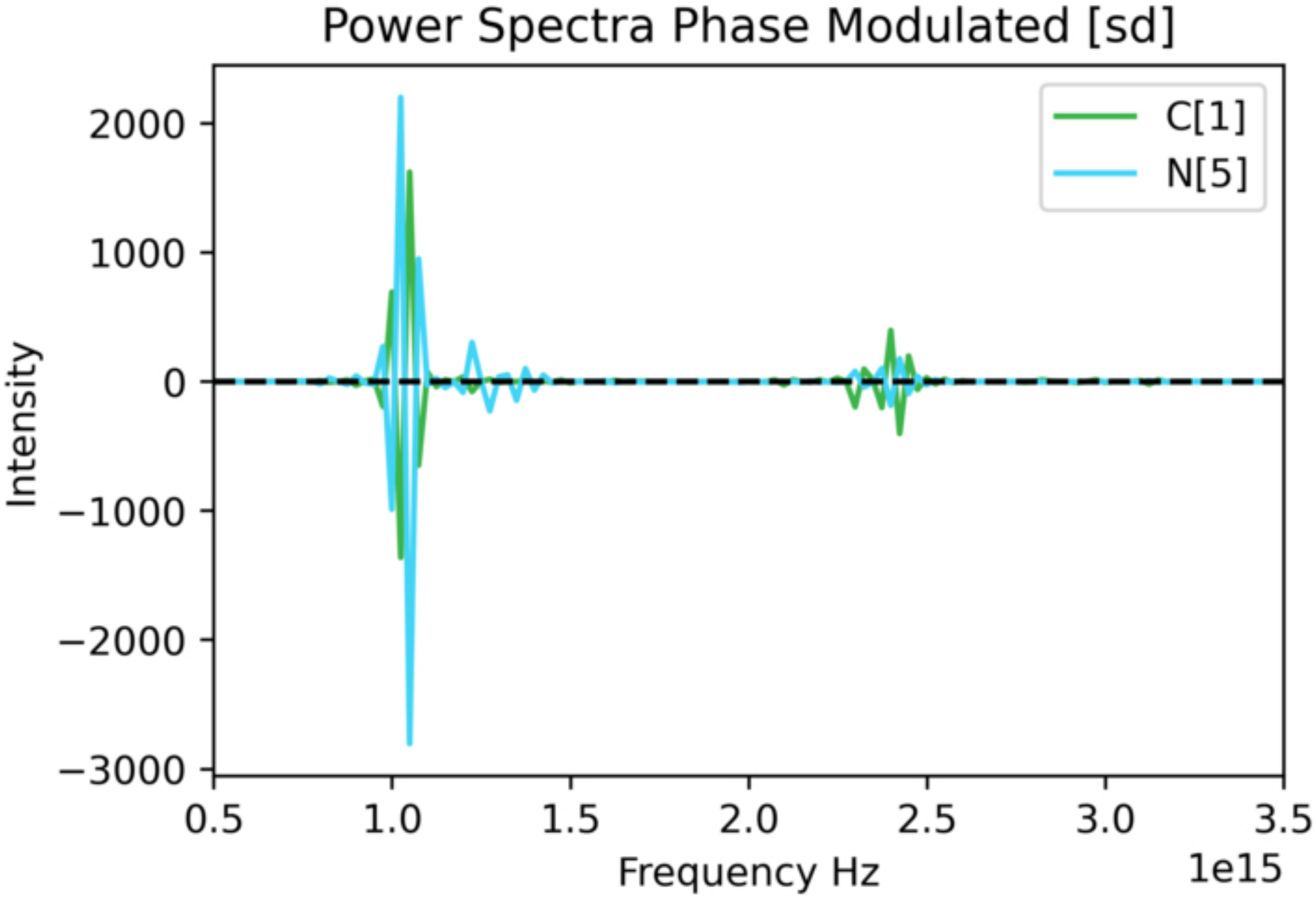
Power Spectra Phase Modulated [sd]
C[1]
N[5]
2000
1000
0
−1000
−2000
−3000
Intensity
0.5
1.0
1.5
2.0
2.5
3.0
3.5
Frequency Hz
1e15

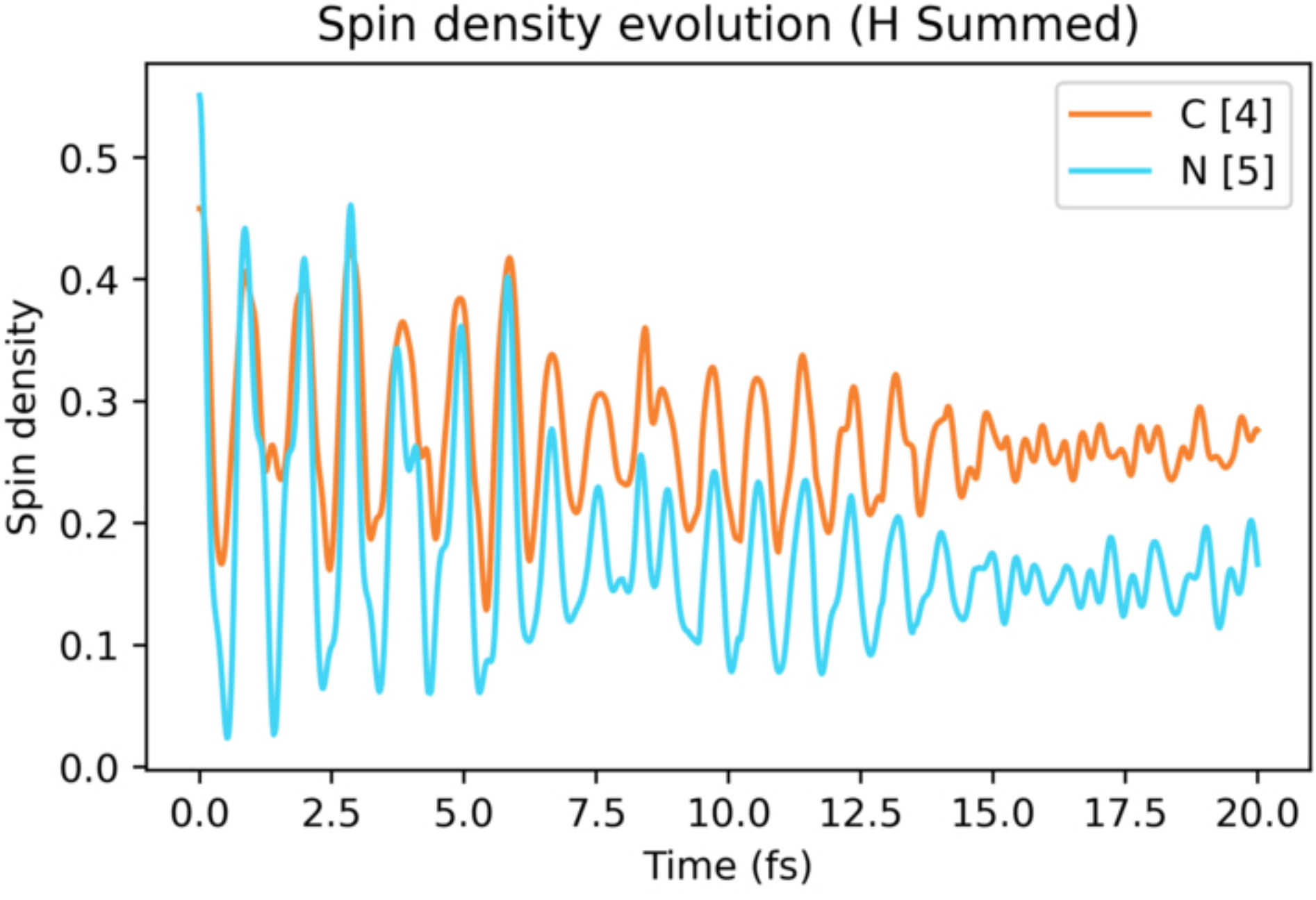
Spin density evolution (H Summed)
C [4]
N [5]
Spin density
0.0
0.1
0.2
0.3
0.4
0.5
0.0
2.5
5.0
7.5
10.0
12.5
15.0
17.5
20.0
Time (fs)

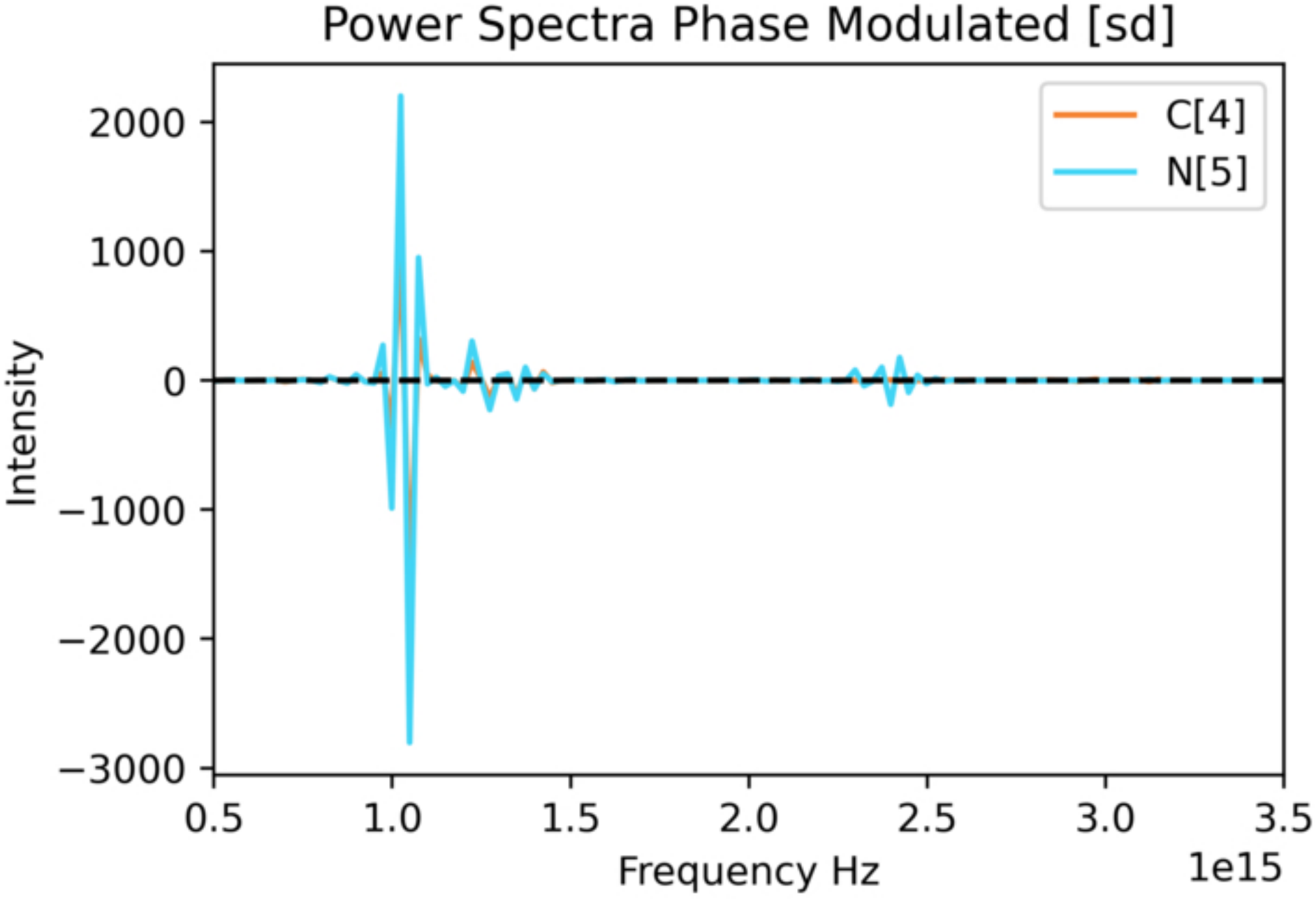
Power Spectra Phase Modulated [sd]
C[4]
N[5]
2000
1000
0
−1000
−2000
−3000
Intensity
0.5
1.0
1.5
2.0
2.5
3.0
3.5
Frequency Hz
1e15

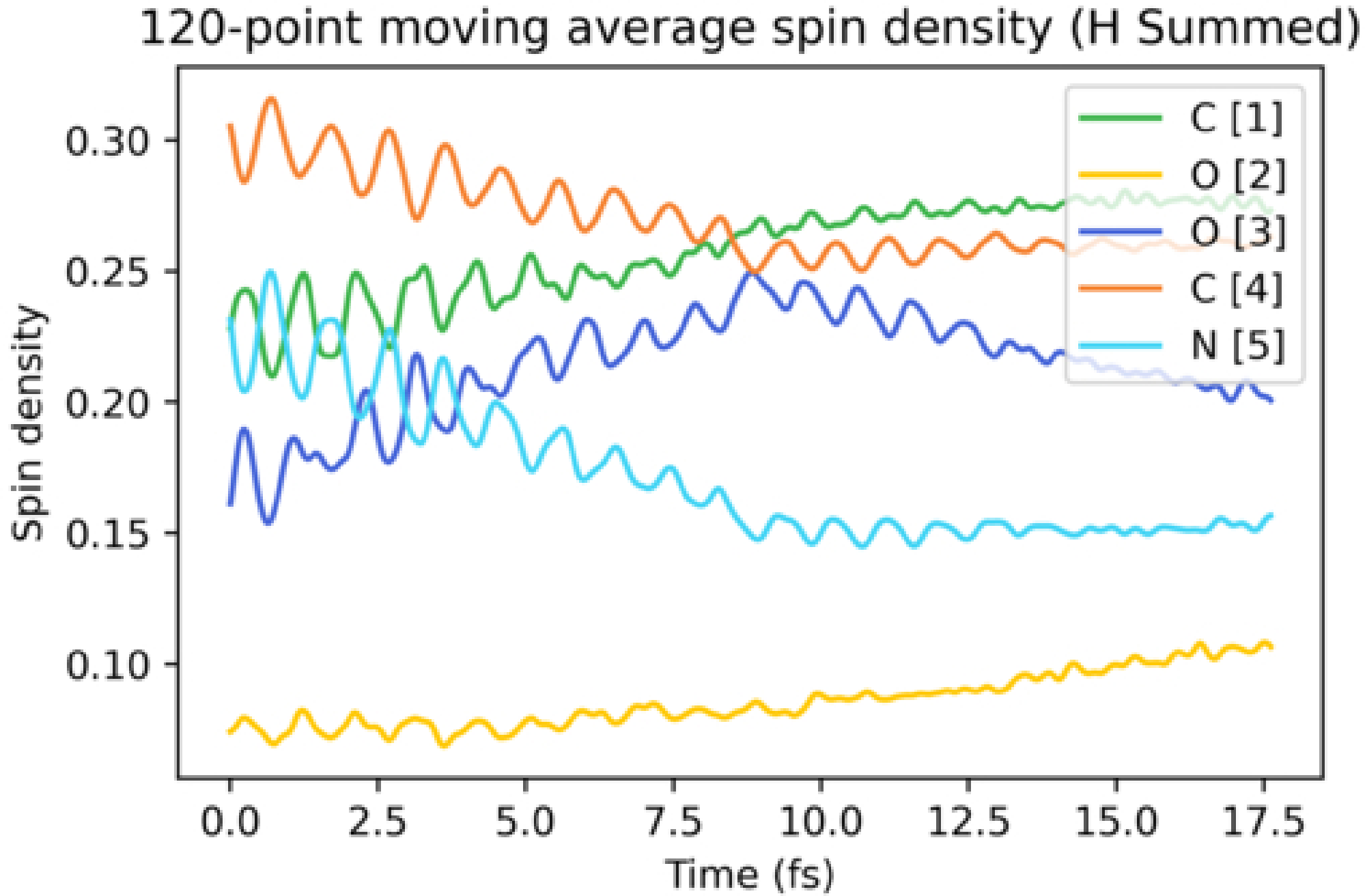
120-point moving average spin density (H Summed)
Spin density
0.30
0.25
0.20
0.15
0.10
0.0
2.5
5.0
7.5
10.0
12.5
15.0
17.5
Time (fs)
C [1]
O [2]
O [3]
C [4]
N [5]